Doctoral Thesis

Layer 1 Projection Diversity of Layer 5 Pyramidal Cells in the Frontal Cortex

Im, Sanghun

The Graduate University for Advanced studies, SOKENDAI

School of Life Science

Department of Physiological Sciences

2020

Contents

Abstract

Behavioral expression and sensory perception require top-down projections from the higher-order areas of frontal cortex to layer 1 (L1) of primary motor and various sensory areas. Within the rodent frontal cortical areas, the secondary motor cortex (M2) has layer 5 (L5) pyramidal cells (PCs) projecting to L1 of diverse neocortical areas. L5 of M2 houses two major PC subtypes: corticopontine (CPn) cells projecting to the pons and intratelencephalic (IT) cells projecting to the contralateral cortex. Both subtypes include PCs that project to other cortical areas, but it remains unclear whether the L1 innervation patterns are differentiated between L5 PC subtypes.

Since L1 houses GABAergic interneurons as well as the apical dendrites of PCs, L5 PCs probably make synaptic connections with these elements. L1 GABAergic cells fall into three classes based on differences in firing pattern, axonal distribution and molecular expression. Therefore, L5 CPn and IT cells may connect differently with L1 GABA cell subtypes.

To elucidate L5 to L1connection properties, which are the key components of the top-down pathway, I investigated the axon distribution of both M2-L5 PC subtypes in L1 and how the subtypes innervate L1 GABA cell subtypes. For selective fluorescent labeling and optogenetic stimulation of L5 pyramidal cell subtypes, I expressed Cre recombinase (Cre) in CPn cells by injecting retrograde AAV virus into the pons and introduced a transgenic mouse line expressing Cre selectively in L5 IT cells (Tlx3-Cre PL56 mouse).

To compare the innervation patterns of CPn and IT cells locally within M2, in the primary motor cortex (M1) and primary sensory cortex (S1), Synaptophysin-tagged EGFP was used to fluorescently label the axon terminals. The terminal boutons of CPn

cells were found more in L1 than layer 2/3 (L2/3) for each cortical area, whereas those of IT cells were quantitatively similar between L1 and L2/3 in M2, but more abundant in L1 for M1 and S1. These suggest that regarding L1 innervation, M2 L5 IT cells have preference for certain cortical areas.

Some L5 IT cells express ER 81 (ETS translocation variant 1), a transcription factor found in cortex.ER81 was expressed in a portion of IT cells projecting to M1 or S1. However, when retrograde tracers were introduced from the axon terminal in L1 of M1 or S1, almost all of the M2-L5 IT cells were positive for ER81. Furthermore, ER81 was expressed in most of L5 IT cells that project to distant areas such as the visual and perirhinal cortex.

Based on these observations, I reasoned that the L1 innervation preference of L5 IT cells is linked to the distal area projection. To investigate this point further, I analyzed the cortical area and layer distributions of axons from individual M2-L5 pyramidal cells found in the MouseLight database of Janelia Research Campus. L1 innervation was diverse in the IT subtype. IT cells with higher innervation to L1 sent more axons to the distal areas than IT cells with lower innervation. Both apical and basal dendrite lengths of the IT cells correlated with the L1 innervation preferences. These findings suggest that L5 IT cells with more abundant L1 innervation have longer dendrites, more axons in the distal cortical areas and higher probability of ER81 expression.

L1 has three subtypes of GABA cells with different physiological characteristics as follows: spike afterdepolarization (ADP cells); spike induction following slowly developing ramp depolarization (late spiking (LS) cells); without ADP and LS (non-ADP/non-LS cells). These physiological subtypes also differed morphologically. Light stimulation of L5 CPn or IT cell axons induced monosynaptic excitation in three L1

subtypes. Input intensities were compared by simultaneous recordings from two cells of different subtypes. EPSC charges induced by L5 IT cell stimulation were similar among the three subtypes. On the other hand, those by CPn cell simulation differed between the postsynaptic subtypes: non-ADP/non-LS cells were the most common, followed by LS cells.

This study revealed that L5 corticocortical pyramidal cells consisted of three groups: CPn cells projecting to the upper L1 of the proximal cortical area; a subpopulation of IT cells with weak L1 innervation and projection to the proximal area; another subpopulation of IT cells with strong L1 innervation and projection to both proximal and distal areas. Connection strength to L1 GABA cells differs between CPn and IT cells. IT cells uniformly excite three L1 subtypes. On the other hand, CPn cells more strongly excite non-ADP/non-LS cells that inhibit the upper part of L1, where the thalamocortical and CPn cell axons are distributed densely. Thus, L5 corticocortical cell subtypes show different connection selectivity in projections to L1, an important pathway of top-down functions.

Introduction

The higher-order areas of frontal cortex receive various kinds of information from sensory areas (bottom-up) and project to primary motor and sensory cortices (top-down) (Barbas and Rempel-Clower, 1997; Shipp, 2005; Yeterian et al., 2012; Barbas, 2015). These top-down signals are important for behavioral expression and sensory perception (Bastos et al., 2012; Shipp et al., 2013; Mejias et al., 2016). In general top-down projections, layer 5 (L5) pyramidal cells (PCs) project to the ipsilateral lower-order cortical areas, especially their layer 1 (L1) (Felleman and Van Essen, 1991; Markov et al., 2014; D'Souza and Burkhalter, 2017). In order to understand the corticocortical top-down actions, it is important to identify what kinds of L5 PCs innervate L1 of other cortical areas and how they select the postsynaptic targets in L1.

Among the frontal cortical areas of rodents, secondary motor cortex (M2) projects to primary motor and diverse sensory areas (Ueta et al., 2014; Manita et al., 2015; Kawaguchi, 2017; Makino et al., 2017). There are two major PC subtypes in M2-L5: corticopontine (CPn) cells projecting to the pons and intratelencephalic (IT) cells projecting to the contralateral cortex. These have different morphological and physiological properties as well as synaptic transmission and connection selectivity (Morishima and Kawaguchi, 2006; Otsuka and Kawaguchi, 2008; Morishima et al., 2011; Kiritani et al., 2012). CPn cell pairs and IT cell pairs have synaptic connections. However IT cells innervate CPn cells unidirectionally (Morishima et al., 2011) (Kiritani et al., 2012). Both CPn and IT project to other cortical areas (Hirai et al., 2012; Ueta et al., 2013; Ueta et al., 2014). Most M2-L5 PCs projecting to the perirhinal cortex (PRC) are IT subtypes, which innervate layer 2/3 PCs (Hirai et al., 2012). However it remains unclear whether the L1 innervation pattern differs between L5 corticocortical PCs. Because L5

IT cells in motor cortex have heterogeneous firing characteristics, dendritic morphology and molecular expression, they may also show diversity in L1 innervation (Otsuka and Kawaguchi, 2011; Ueta et al., 2013; Tantirigama et al., 2014).

L5 PCs probably make synaptic connections with GABAergic interneurons as well as the apical dendrites of PCs in L1 (Palmer et al., 2012; Larkum, 2013a; Ibrahim et al., 2016; Abs et al., 2018; Lam and Sherman, 2019). L1 GABAergic cells fall into several classes based on differences in firing pattern, axon distribution and molecular expression (Hestrin and Armstrong, 1996; Wozny and Williams, 2011; Muralidhar et al., 2013; Schuman et al., 2019). Among them, elongated neurogliaform (eNGF) cells distribute their axons within L1 densely, inhibit PC dendrites through $GABA_A$ and $GABA_B$ receptors, and suppress dendritic Ca^{2+} spikes (Palmer et al., 2012). Another L1 cell group that develops axon collaterals in both L1 and L2/3 (descending cells) inhibits other GABA cells, resulting in disinhibition of L5 PCs (Jiang et al., 2013). The eNGF and descending cells are excited by corticocortical and thalamocortical inputs, causing inhibition and disinhibition at L5 PCs, respectively (Cruikshank et al., 2012; Larkum, 2013b; Ibrahim et al., 2016). Recently eNGF cells have been reported to contain a subpopulation innervating the upper part of L1 and inducing only $GABA_A$ inhibition (canopy cells) (Tasic et al., 2016; Schuman et al., 2019). Therefore, L5 CPn and IT cells may make different connections to the GABA cell subtypes of L1, like those of L5 (Morishima et al., 2017).

To elucidate the L5 to L1 projection characteristics, an important component of the top-down pathway, I investigated the axon distribution of both M2-L5 PC subtypes in L1, and how they affect synaptic connection to L1 GABA cell subtypes. The results showed that L5 IT cells were more heterogeneous in L1 innervation patterns than CPn

cells: some IT cells with L1 innervation preference projected extensively to both proximal and distal areas, whereas others with lower L1 innervation preference mainly innervated the proximal areas such as primary motor area, similar to CPn cells. CPn cells induced subtype-dependent excitation of postsynaptic L1 GABA cell more than L5 IT cells. Thus, the L5 PC subtypes differed not only in connection selectivity within L5 but also in the projection to L1, which is involved in top-down functionality.

Materials and Methods

Animals

The following mouse lines were used for morphological and electrophysiological analysis: ICR (Japan SLC); Tlx3-Cre PL56 (Tlx3; MGI: 5311700) expressing Cre recombinase (Cre) in L5 IT cells (Gerfen et al., 2013); Ai14 (Rosa-lsl-tdTomato; MGI: 3809524) used for Cre reporter (Madisen et al., 2010); VGAT-tdTomato (Line 54) expressing tdTomato in GABAergic cells (Kaneko et al., 2018). The following primers were used for PCR genotyping: 5′-GAAAGATGACACAGAGCCTGTCGGG-3′ and 5′-CGGCAAACGGACAGAAGCATT-3′ for Tlx3; 5′-CTGTTCCTGTACGGCATGG-3′ and 5′-GGCATTAAAGCAGCGTATCC-3′ for Ai14; 5′-AAGAGATTGCATGGACCTT
GG-3′ and 5′-TCCAGCATATAACAGCACCAG-3′ for VGAT-tdTomato. The PCR products were amplified by Premix Taq Hot Start Version (TAKARA, RR030A). Red fluorescence was detected through the cephalic skin in tdTomato-expressing mice which are the progeny of Tlx3 crossed with Ai14 (Tlx3-Ai14). All experiments were conducted in compliance with the guidelines of the Institutional Animal Care and Use Committee of the National Institutes of Natural Sciences.

Retrograde labeling of PCs

Mice were anesthetized with a mixture of ketamine (40 mg/kg, intramuscular [i.m.]) and xylazine (12 mg/kg, i.m.), followed by injections of glycerol (0.6 g/kg, intraperitoneal injection [i.p.]) and dexamethasone (3.5 mg/kg, i.p.). After the animals were placed in a stereotaxic apparatus, one of the following retrograde tracers was injected into individual regions (Table 1) by pressure injection (PV820 Pneumatic

PicoPump) through glass pipettes (tip diameter, 40-60 µm; approximately 100 nl): Alexa Fluor 647-conjugated cholera toxin subunit B (CTB-647; Life Technologies Corporation, C34778; 0.2% in distilled water or phosphate buffered saline); red fluorescent RetroBeads (Lumafluor). For injection into perirhinal cortex including ectorhinal cortex and temporal area cortex, the pipette was positioned at a 30° lateral inclination (Hirai et al. 2012; Ueta et al. 2013). For retrograde labeling from L1 axonal fibers, a filter paper (~1 mm^2) soaked with Fast Blue (FB; Dr. Illing GmbH and Co. KG, Groß-Umstadt, Hesse, Germany; 2% in distilled water) were placed on the pia for ~5 min, followed by saline wash (Rubio-Garrido et al., 2009). After a survival period of 4-7 days, the mice were deeply anesthetized with isoflurane and perfused transcardially with a prefixative (250 mM sucrose and 5 mM $MgCl_2$ in 0.02 M phosphate-buffer (PB) solution, pH ~7.4) followed by a fixative (4% paraformaldehyde and 0.2% picric acid in 0.1 M PB solution). The brains were postfixed in fixative solution for 2 h at room temperature.

Virus injection for axon labeling and optogenetic stimulation

After induction of anesthesia as described above, this state was maintained by isoflurane (0.25-0.5%) via inhalation. For induction of Cre in CPn cells, AAV 2.retro pgk-Cre (Addgene viral prep # 24593-AAVrg; Patrick Aebischer Lab unpublished) was injected into the pons. For fluorescence labeling of Cre-induced somata and axons, AAV 2.5 CAG Double flox Synaptophysin-EGFP WPRE (Addgene #73816) (Harwell et al., 2012) was prepared by Helper Free Expression System (Cell Biolabs, Inc., San Diego, CA, USA) and injected into M2 (~50 nl). For optogenetic stimulation of Cre-induced cells, AAV 2.5 pAAV-EF1a-double floxed-hChR2(H134R)-mCherry-WPRE-HGHpA (Addgene viral prep # 20297-AAV5; Karl Deisseroth Lab unpublished) was injected into

two locations in M2 (~200 nl in total). After a survival period of 3-5 weeks, these mice were perfused with the fixative, or used for in vitro electrophysiological experiments.

Histological identification of cortical areas, layers and cell subtypes

The perfusion-fixed brains were cut into 20-µm-coronal or sagittal sections using a vibratome (Leica Microsystems, VT1000S). As primary antibodies, a mouse monoclonal antibody against the neurofilament heavy chain (anti-NF-H; Sigma-Aldrich Co. LLC, N0142; 1:2000) was used for area identification of M2 and a guinea pig polyclonal antibody against vesicular glutamate transporter type 2 (anti-VGluT2; Merck, AB2251; 1:2000) was used for layer identification in M2. A mouse monoclonal antibody against vertebrate neuron specific nuclear protein (anti-NeuN; Merck, MAB377; 1:1000), a rabbit polyclonal antibody against ER 81 (ETS translocation variant 1) (anti-ER81 from Thomas Jessell; 1:20000) (Arber, Ladle et al. 2000) and a rat monoclonal antibody against chicken ovalbumin upstream promoter transcription factor-interacting protein 2 (anti-Ctip2; Merk, AB18465; 1:1000) were used for cell subtype identification. Sections were incubated overnight at 4°C with the primary antibodies in 0.05 M Tris-buffered saline (TBS) containing 10% normal goat serum, 2% bovine serum albumin and 0.5% Triton X-100. Anti-Ctip2 incubation was performed in Can Get Signal immunostain Solution B (TOYOBO, NKB-601) for ~2 h at room temperature.

Subsequently fluorescence secondary antibodies were used: Alexa Fluor 350 for NeuN; Alexa Fluor 488 or 594 for anti-VGluT2; Alexa Fluor 488 for anti-ER81; Alexa Fluor 594 or 647 for anti-Ctip2; Alexa Fluor 633 for NF-H. The sections were mounted on glass slides, coverslipped with antifade solution (Thermo Fisher Scientific, ProLong Gold, P36934), observed with an epifluorescence microscope (Olympus, IX-83), and

analyzed by Neurolucida (MBF Bioscience) and IGOR Pro software (WaveMetrics). Brightness and contrast of fluorescent image were adjusted using Adobe Photoshop

Analysis of anterogradely labeled axons

The density of Synaptophysin-EGFP-labeled puncta, putative axon terminals, was manually counted in a 50-μm-wide image of L1 and a part of L2/3 (the same thickness as L1 from L1/2 border, 105 ± 60 μm). Laminar distribution index of L1/2/3 was defined as the difference between L1 and L2/3 puncta densities divided by their sum in individual sections. Laminar distribution index of L1 was defined from L1a and L1b puncta densities.

Morphological analysis using the MouseLight database

Morphological data of L5 PCs in M2 were downloaded from the MouseLight database (http://ml-neuronbrowser.janelia.org/, Janelia Research Campus). Cell position was confirmed to be L5 of M2 using Allen Mouse Common Coordinate Framework (CCFv3) (http://help.brain-map.org/display/mousebrain/API) (Kuan et al., 2015). Note that L5 IT cells were defined as L5 cells projecting to the contralateral neocortex.

The axon length was the summation of Euclidean distances between neighboring points. An 'end-point' was defined as a point without further continuation. The axon length and end-point number were obtained for individual cortical areas and respective layers by referring to the atlas information from AllenID which includes both ipsi- and contra- information.

For dendrite analysis, I excluded AA0324, AA0646, AA0841, AA0905 and AA0907 because of difficulty in identifying apical dendrites. The morphologies were

analyzed by the custom-made codes in Image J (NIH), MATLAB (MathWorks), Ruby (https://www.ruby-lang.org/ja/) and Microsoft Excel (Microsoft).

In vitro electrophysiological recording and analysis

Mice of both sexes at postnatal day 42-56 were deeply anesthetized with isoflurane, and transcardially perfused with cooled NMDG buffer containing (in mM): 90 N-methyl-d-glucamine (NMDG), 40 choline chloride, 2 KCl, 1.25 NaH_2PO_4, 1.5 $MgCl_2$, 0.5 $CaCl_2$, 26 $NaHCO_3$, 10 glucose and 0.2 ascorbic acid (pH 7.3-7.4 adjusted with HCl) equilibrated with a mixture of 95% O_2 and 5% CO_2 (~330 mOsm). After the brain was quickly removed, the block containing M2 was sliced into 300-μm-thick oblique horizontal sections in the NMDG buffer by vibratome. Slices were immersed for 20 min at 32 ˚C, followed by incubation at room temperature longer than 1 h in an artificial cerebrospinal fluid (ACSF) containing (in mM): 124 NaCl, 3 KCl, 2.4 $CaCl_2$, 1.2 $MgCl_2$, 26 $NaHCO_3$, 1 NaH_2PO_4, 10 glucose, 3 pyruvic acid and 0.2 ascorbic acid. Recordings were made in the whole-cell mode (Molecular Devices, Multiclamp 700B) at 30 ± 1°C, using infrared differential interference contrast microscopy (IR-DIC; Olympus, BX50WI) with CCD camera (Hamamatsu, ORCA-R2). Pyruvic acid and ascorbic acid were omitted from the solution used for recordings. I performed recording from L1 cells, but not cells distributed in the L1/L2 border. The pipette solution for both current-clamp and voltage-clamp recordings contained (in mM): 130 potassium gluconate, 2 KCl, 2 $MgCl_2$, 3 ATP-Na_2, 0.3 GTP-Na, 10 HEPES and 0.5-0.75% biocytin (~295 mOsm, pH 7.3-7.4 adjusted with KOH). Intrinsic membrane properties were analyzed only in recordings with series resistances lower than 35 MΩ. In current clamp recording, the bride balance was adjusted accordingly. The liquid junction potential was not corrected.

For classification of L1 cells, the membrane potential change and spike discharge patterns in response to rheobase current (duration, 1 s) were analyzed in detail. A late spiking (LS) pattern was identified by firing delay and slope of ramp depolarization by the threshold current, detected by current increments of 5 pA. The delay time was measured from the current pulse start to spike onset. To confirm the ramp depolarization, the membrane potential slope was measured from 110 to 10 ms prior the spike onset. I measured the delay time just at the rheobase several times by adjusting the current strength by 1 pA. When the delay time was longer than 150 ms and the slope was larger than 5 mV/s, I regarded this as the LS pattern induced by the ramp depolarization.

An amplitude of afterdepolarization (ADP) following a spike with afterhyperpolarization (AHP) was tentatively quantified as voltage difference between the AHP trough and the highest potential within 4 ms from the trough. When this amplitude was larger than 0.02 mV and reduced to more than half within 20 ms, I accepted this transient depolarization as ADP. Then, I measured the ADP amplitude just at the spike threshold several times.

Membrane time constant and input resistance were measured by applying hyperpolarizing current pulses (-20pA, 1s). Depolarizing humps were induced at a current strength around the spike threshold, where the hump with or without a spike occurred equally. In the humps without any spike, I measured the voltage difference between the maximum potential within 200 ms from the onset and the average potential during the latter half (500 ms) of the current pulse. The maximum difference was used from repetitions as hump amplitude. Hyperpolarizing sags were induced by hyperpolarization to around -30 mV from resting membrane potential (Vrest). The sag amplitude (%) was defined as follows: ((Vsteady – Vsag-peak) / (Vrest – Vsteady) × 100); Vsteady, averaged

potential in the latter half of current pulse (duration: 500 ms); Vsag-peak, the peak of hyperpolarization. A mean of sag amplitude induced by two current pulses (50 pA difference) was used for the analysis.

F/I Slope (Hz/nA) was calculated by linear regression of the relation between action potential firing frequency (F) and injected current intensity (I), which was obtained by application of depolarizing current pulses, started from +300 pA (1 s), decremented by 50 pA. When the spike number was fewer than 20 at +300 pA, depolarization was restarted from +500 pA. Electrophysiological data were analyzed by IGOR Pro and Microsoft Excel.

Morphological analysis of recorded cells

Slices containing biocytin-labeled cells were placed in a fixative longer than 3 h at room temperature (4% paraformaldehyde in 0.1 M PB). To know the soma position in L1, the slices were incubated with Alexa Fluor 488 conjugated streptavidin (Thermo Fisher Scientific, S11223) in TBS containing 5% tritonX-100 for longer than 4 h at room temperature. The fluorescent images of somata were overlapped with the bright field image for identification of L1/2 border in TBS. The 7 slices were re-sectioned in to 50-μm-thickness and stained with anti-VGluT2 antibody. L1a was stronger in VGluT2 immunoreactivity than L1b.

For analysis of cell morphology, after incubation in 0.001% H_2O_2, the slices were further re-sectioned into 50-μm-thickness. The sections were incubated overnight at 4°C with 1% avidin-biotin-peroxidase complex (ABC elite; Vector Laboratories, PK-6100) in TBS containing 0.5% Triton X-100. After wash in TBS, the sections were reacted with 0.05% 3, 3'-diaminobenzidine tetrahydrochloride and 0.001% H_2O_2 in 0.05 M Tris-HCl

buffer. The sections were then further fixed in 0.1 M PB containing 1% OsO_4 and 7% glucose, dehydrated, and embedded in Epon on glass slides. Bright field images of a recorded cells were captured by 1-μm-z-steps and stitched seamlessly (Olympus, IX-83). The dendrites and axons were reconstructed from these three-dimensionally connected images using Neurolucida. The section thickness error due to a refractive index in image capture was corrected.

Photostimulation

To excite axons of the ChR2 loaded neurons, I irradiated blue light (LED; Thorlabs, M470L3) controlled by a driver (Thorlabs, LEDD1B) through 40× water immersion lens and mirror unit for GFP (Olympus, U-MWIB2). The irradiation time was 1 ms; intensities were 1.8-11.8 mW measured at the recording chamber. EPSC recordings were performed by holding the cell at -60 mV. The stimulus intensity was adjusted to the minimum to record EPSCs by inserting a neutral density filter (25% or 6%) in the light path. I recorded photo-induced EPSCs after confirming no action potential was elicited in the presence of 0.5 μM tetrodotoxin (TTX; Latoxan, L8503) and 1 mM 4-Aminopyridine (4-AP; Sigma, 275875) (Petreanu et al., 2009). Photostimulation was applied ten times at an interval of 30 s. The excitatory synaptic charge (SC) was obtained by temporal integration of the EPSC from stimulus onset to 100 ms later. To compare excitation differences between two simultaneously recorded cells, I calculated SC index: SC differences between the two cells divided by the sum of their SCs.

Statistical analysis

Data are presented as mean ± standard deviation (SD). I performed D'Agostino-

Pearson normality test to determine whether the data followed normal distribution or not. The morphological deference between the two PC subtypes was tested by unpaired t test for normally-distributed data and Mann Whitney test for non-normally-distributed data. The innervation differences among cortical areas and the soma location differences among L1 subtypes were tested by one-way ANOVAs and post-hoc Tukey's multiple comparison test. The physiological differences among L1 cell subtypes were tested by Kruskal-Wallis and post hoc Dunn's multiple comparison tests. The difference from the reference was tested by the one sample t test. The correlation was tested by Pearson correlation for normally-distributed data and Spearman correlation for non-normally-distributed data. Statistical examination was performed using GraphPad Prism 8 (GraphPad). Significance was accepted when $P < 0.05$.

Results

L1 axonal distributions of M2-L5 pyramidal cells

In M2, both L5 IT and CPn cells locally send axon collaterals up to L1 with different sublayer distributions (Hirai et al., 2012). Furthermore, M2 innervates L1 of other cortical areas (Ueta et al., 2013). Therefore, I investigated whether the L1 innervation pattern in each area is also different between M2-L5 IT and CPn cells.

For selective labeling and manipulation of L5 IT cells, I utilized a Tlx3-Cre PL56 (Tlx3) mouse line (Gerfen et al., 2013). L5 is divided into upper L5a and lower L5b: L5b is more positive for VGluT2, which is marker of axonal terminal from thalamus, than L5a (Fig. 1A) (Morishima et al., 2011). Cre-expressing cells in Tlx3 mice (Tlx3 cells), labeled fluorescently by crossbreeding with Ai14 mice, were distributed predominantly in L5a (Fig. 1A 'Ai14'). Tlx3 cells labeled fluorescently by local virus injection were also found more in L5 (Fig. 1A 'AAV'). CPn cells were labeled retrogradely from pontine nuclei. One out of 196 L5a CPn cells, and none of 358 L5b CPn cells overlapped with Tlx3 cells (3 mice; Fig. 1B). This confirmed that L5 Tlx3 cells were distinct from CPn cells.

For selective labeling and manipulation of CPn cells, Cre was selectively expressed by retrograde virus transportation from the pontine nuclei. For fluorescent axon labeling of PC subtypes, FLEX Synaptophysin-EGFP, more preferentially distributed in axons/somata than dendrites, was introduced into M2 cells using virus (Fig. 2) (Harwell et al., 2012). The fluorescent puncta were considered as putative synaptic boutons of axons (Fig. 3A). The L1 and L2/3 innervation difference was represented by the laminar distribution index: the difference in the density of fluorescent puncta between L1 and L2/3, divided by their sum (+1: distribution only in L1; -1: only in L2/3).

In M2, CPn cells preferentially innervated L1 (laminar distribution index = 0.48

± 0.12, 3 mice, $P = 0.020$, one sample t test, hypothetical value = 0), whereas Tlx3 cells innervated L1 and L2/3 more uniformly (index = -0.066 ± 0.104, 3 mice, $P = 0.39$) (Fig. 3B).

In the corticocortical target areas, CPn cell axons were distributed more in L1 than L2/3 of primary motor (M1; index = 0.84 ± 0.17, $P = 0.014$) and of primary sensory cortices (S1; index = 0.93 ± 0.01, $P = 0.0021$); Tlx3 cell axons were also distributed more in L1 of M1 (index = 0.50 ± 0.10, $P = 0.012$) and S1 (index = 0.52 ± 0.06, $P = 0.038$). CPn cells had a higher innervation preference for L1 compared to L2/3 than Tlx3 cells in each area (M2, P = 0.0039; M1, $P = 0.043$; S1, $P = 0.0016$; unpaired t test; Fig. 3B).

In both CPn and Tlx3 cells, the L1 and L2/3 innervation pattern was different between local M2 and target areas ($P = 0.011$ for CPn cells and $P = 0.0003$ for Tlx3 cells, ordinary one-way ANOVA). L1 innervation preferences of M2 cells was higher in M1 and S1 than in M2 local (M2 vs. M1: $P = 0.032$ for CPn and $P = 0.0005$ for Tlx3; M2 vs. S1: $P = 0.0004$ for CPn and $P = 0.012$ for Tlx3; post hoc Tukey's multiple comparisons test).

L1 is divided into two sublayers, upper L1a and lower L1b with higher and lower immunoreactivity for VGluT2, respectively. CPn cell axons were distributed more in L1a than in L1b in each area (M2, $P = 0.0008$; M1, $P = 0.019$; S1, $P = 0.0033$; one sample t test). CPn cells had a higher innervation preference of L1a compared to L1b than Tlx3 cells in each area (M2, $P = 0.037$; M1, $P = 0.97$; S1, $P = 0.28$; unpaired t test) (Fig. 3C). These results suggest that M2 CPn cells innervate more L1, especially L1a, than L2/3 commonly throughout the local and target areas, but M2-L5 IT cells exhibit area-dependent preferences for L1 innervation.

Correlation of ER81 expression with L1 innervation and distal area projection in L5 IT cells

L5 PCs are heterogeneous in molecular expression pattern (Molyneaux et al., 2009; Tasic et al., 2018). Among those molecules, ER81 (*Etv1*: ETS translocation variant 1) is expressed in a proportion of IT cells (Yoneshima et al., 2006; Harb et al., 2016). I confirmed that ER81-positive cells were distributed in L5 of M2, especially in L5a (Fig. 4A), where more corticocortical (CC) cells are found than in L5b (Fig. 4B) (Ueta et al., 2013). Furthermore, ER81 was expressed in 73.4% of Tlx3 cells (482 out of 656 cells, 3 mice; Fig. 4C top). I validated this point by observing that some of the contralateral M2-projecting cells (cM2p; IT type) expressed ER81 in L5a, but very few of them were observed in L5b (Fig. 4C middle and bottom). Since Tlx3 cells exhibited different layer distributions of axons between the local and target areas (Fig. 3B). I investigated the innervation pattern of ER81-positive IT cells to correlate the molecular and innervation diversity among L5 IT cells.

For separation of L5 IT and CPn cells among CC cells, Ctip2 expression can be used (Arlotta et al., 2005; Ueta et al., 2014). In M2, CPn cells labeled retrogradely from the pons were all positive for Ctip2 in both L5a (196 cells, 3 mice; Fig. 5A top) and L5b (358 cells). In Tlx3 cells (IT type), only 1.3% of the population in L5a was Ctip2 positive (4 out of 309 cells, 3 mice; Fig. 5A middle) whilst 24.7% of the population in L5b was found to be positive (18 out of 73 cells). In cM2p cells (IT type), only 1.5% of the population in L5a was Ctip2 positive (3 out of 194 cells, 3 mice; Fig. 5A bottom). However 62.3% of the population in L5b was found to be positive (142 out of 228 cells). These findings suggest that Ctip2 is selectively expressed in CPn cells in L5a and can be used for separating L5a PC subtypes. In addition, PCs could be identified as neurons

positive for NeuN immunostaining other than fluorescent GABAergic cells in VGAT-tdTomato mice (Kaneko et al., 2018). Therefore, L5a IT cells could be identified as non-GABAergic neurons negative for Ctip2 (proportion of IT cells among PCs = 64.0%, n = 1126, 3 mice; Fig. 5B). ER81was expressed in 57.2 ± 3.3% of L5a IT cells (n = 709, 3 mice; Fig. 5C). L5 PRCp IT cells have different firing properties than with M1p IT cells (Hirai et al., 2012; Ueta et al., 2013), so I investigated ER81 expression for each corticocortical IT type. With layer-nonselective injection of retrograde tracers into target areas (Fig. 6A 'CTB'), ER81 was expressed in most of L5a IT cells projecting to the perirhinal cortex (PRC; 93.4 ± 0.7%, n = 236, 3 mice) and to the visual cortex (Vis; 96.8 ± 2.8%, n = 57, 3 mice), but only partially in those projecting to M1 (65.9 ± 1.4%, n = 113, 3 mice) and to S1 (64.3 ± 6.3%, n = 401, 3 mice) (Fig. 6B top, C white bars). In this study most ER81 negative IT cell innervations were restricted in M1 and S1. Tlx3 cells exhibited different L1 distributions of axons according to innervated areas (Fig. 3B). I reasoned that ER81 expression might be related to the L1 innervation pattern differences. Thus, I investigated whether ER81-postive and -negative cells were different in L1 innervation strength. M1 and S1 projecting IT cells are retrogradely labeled M2-L5a IT cells projecting to L1 of M1 or S1, by applying a retrograde tracer (FB: Fast blue) just onto their cortical surface (Fig. 6A 'FB'). In contrast with M2 IT cells labeled by the layer-nonselective injection, those labeled by L1 tracer application were mostly positive for ER81 both in M1 (92.5 ± 6.5%, n = 95, 3 mice) and S1 (90.9 ± 1.2%, n = 219, 3 mice) (Fig. 6B bottom, C gray bars). These results suggest that M2-L5a IT cells projecting to M1 and S1 are more heterogeneous than those projecting to PRC and Vis: ER81-positive cells have more axons in L1 while ER81-negative cells have fewer axons in L1.

Correlation of L1 innervation preferences with distal area projections in L5 IT cells

The above analysis revealed that M2-L5 IT cells with more L1 innervations or richer projections to the distal areas are positive for ER81. To further examine the projection pattern of individual L5 IT cells, I utilized the whole brain reconstruction data of L5 PCs, provided by (Janelia Research Campus) through their MouseLight project (http://ml-neuronbrowser.janelia.org/) (Economo et al., 2016; Winnubst et al., 2019). From this database 79/998 cells are M2-L5 PCs and 69 cells were situated in M2 as defined in the Allen atlas (Kuan et al., 2015). I excluded neurons that neither project to contralateral cortex nor pons (14 cells). The distribution of axons from 39 IT cells and 16 CPn cells was analyzed. I calculated the axonal length and end-points in individual target areas and layers. The end-points can be a good proxy for the density and spatial distribution of synapses (Morita et al., 2019). Some PCs did not blanch in neocortex in this date set. In the PCs innervating L1, the shortest total length of axons in L1 and L2/3 (L1/2/3) was 1308 μm. PCs with axon lengths in L1/2/3 longer than this value could possibly innervate L1, and were used for further analysis (37 IT and 5 CPn cells; Table2).

To quantify the L1 innervation preference, I calculated the proportions of axonal length and end-points in L1 to those in L1/2/3 (L1 length ratio and L1 end-points ratio, respectively). These two ratios were well correlated (R = 0.75, P < 0.0001, Pearson correlation), and diverse especially among IT cells (Fig. 7A). L1 length ratio was smaller in IT cells (0.22 ± 0.16) than in CPn cells (0.48 ± 0.26; P = 0.0032, unpaired t test) (Fig. 7A). L1 end-point ratio was also smaller in IT cells (0.43 ± 0.25) than in CPn cells (0.81 ± 0.16; P = 0.0024). Some IT cell had similar L1 length/end-points ratios to CPn cells (Fig. 7A arrow, Fig. 7B), while some IT cells innervate to L1 less than CPn cells (Fig. 7A arrowhead, Fig. 7C).

I wondered if L1 innervation diversity among L5 IT cells was related to the target cortical area. Thus, I compared the L1 innervation patterns among target areas in individual M2 IT cells. The L1 axonal length ratio in M2 was correlated with that in M1 (R = 0.53, P = 0.0053, Spearman correlation; Fig. 8A) and in S1 (R = 0.59, P = 0.049; Fig. 8B). This suggests that L1 innervation preference of each M2-L5 IT cell is persevered among the target cortical areas. Both y-intercepts of regression lines were positive (M2-M1: y = 0.80 x + 0.15, M2-S1: y = 0.36 x + 0.31; Fig. 8AB). Since this suggests that L1 innervation preference is higher in M1 and S1 than M2 local, I compared L1 innervations between M2, M1 and S1. L1 axonal length ratios of L5 IT cells were higher in M1 and S1 than in M2 (Fig. 8C; P = 0.0036, Kruskal-Wallis test; P = 0.26 for M1 vs. M2 and P = 0.011 for S1 vs. M2, *post hoc* Dunn's multiple comparisons test; Fig. 8C). As in Tlx3 cell axonal boutons (Fig. 3B), these observations suggest that L1/2/3 of M2 are innervated more uniformly by diverse M2-L5 IT cells than those of other areas.

Previously, IT cells projecting to distal areas were ER81 positive (Fig. 6). Therefore PRC or Vis projecting IT cells might highly innervate L1. I analyzed the relationship between L1 innervation preferences in M2 and the other areas in individual L5 IT cells. The total axon length in the proximal areas (M1 and S1) was independent of the L1 axonal length ratio in M2 (R = 0.0037, P = 0.98; Fig. 8D), which suggests that these areas are innervated by diverse M2-L5 IT cells. In the distal areas (PRC: Perirhinal area, Ectorhinal area and Temporal association areas; Vis: Primary visual area, Anterolateral visual area, Anteromedial visual area, Lateral visual area, Laterointermediate area, Posterolateral visual area, Posteromedial visual area and Postrhinal area), on the other hand, the two parameters were positively correlated (R = 0.40, P = 0.022; Fig. 8E), which suggests that M2-L5 IT cells with L1 innervation

preference send more axons to the distal areas. Then I investigated whether dendritic morphologies were also differentiated together with the axonal differences. L5 IT cells are diverse in dendritic morphologies, correlated with their physiological and molecular properties (Otsuka and Kawaguchi, 2008; Tantirigama et al., 2014). Total length of apical and basal dendrites were well correlated with L1 axonal length ratio (apical: $R = 0.38$, $P = 0.031$; basal: $R = 0.48$, $P = 0.0053$; Fig. 9A). The dendritic lengths were independent of total axonal length in neocortex (apical: $R = 0.21$, $P = 0.25$; basal: $R = 0.24$, $P = 0.19$; Fig. 9B). These findings suggest that L5 IT cells with preferential L1 innervation develop longer apical and basal dendrites. Taking into consideration that ER81 was expressed more in L5 IT cells innervating L1 prferentially and in those projecting to the distal areas (Fig. 8), these analyses suggest that L5 IT cells are heterogeneous in L1 innervation preference which is correlated with distal projections, dendrite extension and ER 81 expression.

Identification of three classes of L1 GABA cells

In M2, L1 was innervated by CPn cells and by IT cells projecting to both proximal and distal areas. I examined whether L5 CPn and IT cells exhibited different connection selectivity with L1 GABA cells, as they do with L5 GABA cells reported previously (Morishima et al., 2017). For this, I confirmed three class of L1 interneurons based on electrophysiological and morphological properties as reported previously in S1 (Schuman et al., 2019). The first class showed afterdepolarization (ADP) following initial spike with short afterhyperpolarization in response to suprathreshold depolarization (ADP cell; Fig. 10A left). ADP amplitude was larger in ADP cells (3.01 ± 2.42 mV, n = 38) than in the other classes (0.00 ± 0.01 mV for LS cells (n = 13); 0.02 ± 0.04 mV for non-

ADP/non-LS cells (n = 45); $P < 0.0001$, Kruskal-Wallis test; $P < 0.0001$ for ADP cells vs. LS cells and $P < 0.0001$ for ADP cells vs. non-ADP/non-LS cells, post hoc Dunn's multiple comparisons test; Fig. 10B 'ADP'). The second class had ramp depolarization from 110 to 10 ms prior the initial spike onset (late spiking: LS; 34.6 ± 16.4 mV/s, n = 13) at rheobase (LS cell; Fig. 10A center). Spike induction latency from the onset of current pulse was longer in LS cells (360.4 ± 122.6 ms, n = 13) than in the other classes (38.7 ± 23.2 ms for ADP cells (n = 38), 46.1 ± 38.3 ms for non-ADP/non-LS cells (n = 45); $P < 0.0001$, Kruskal-Wallis test; $P < 0.0001$ for LS cells vs. ADP cells and $P < 0.0001$ for LS cells vs. non-ADP/non-LS cells; Fig. 10B 'Delay'). The third class was identified by no ADP and no LS characteristics (non-ADP/non-LS cell; Fig. 10A right). ADP cells had larger depolarizing humps just below threshold depolarization (4.89 ± 2.26 mV) than the other classes (3.05 ± 1.89 mV for LS cells and 3.20 ± 1.97 mV for non-ADP/non-LS cells; $P = 0.0008$, Kruskal-Wallis test; $P = 0.037$ for ADP cells vs. LS cells and $P = 0.0012$ for ADP cells vs. non-ADP/non-LS cells; Fig. 10B 'Hump'), and also larger hyperpolarizing sags (14.6 ± 10.8%) than the other classes (3.33 ± 1.38% for LS cells and 4.83 ± 3.27% for non-ADP/non-LS cells (n = 45); $P < 0.0001$, Kruskal-Wallis test; $P < 0.0001$ for ADP cells vs. LS cells and $P < 0.0001$ for ADP cells vs. non-ADP/non-LS cells; Fig. 10B 'Sag'). There were no significant differences in other intrinsic properties: resting potential, input resistance, time constant and F/I slope (Table 3)

The morphological differences among the three classes were compatible with those described in the previous report (Schuman et al., 2019): ADP cells have horizontal axonal arbors with descending axon collaterals (descending cell; Fig. 11A left); LS cells correspond to elongated neurogliaform cells with axonal arbors within L1 (eNGF cell; Fig. 11A center); non-ADP/non-LS cells extend axons within L1, especially at the upper

half of L1 (canopy cell; Fig. 11A right) (Schuman et al., 2019). The soma positions of ADP cells and LS cells were biased to the lower half of L1 (ADP cells, $P = 0.0020$; LS cells, $P = 0.048$; non-ADP/non-LS, $P = 0.82$, one sample t-test, hypothetical value = 0.5). However the soma positions of three subtypes were biased to the L1b (ADP cells, $P < 0.0001$; LS cells, $P < 0.0001$; non-ADP/non-LS, $P < 0.0001$, one sample t-test, hypothetical value = 0.3781) and the soma distribution along L1 depth was not different among the three classes ($P = 0.45$, ordinary one-way ANOVA; ADP cells vs LS cells, $P = 0.98$; ADP cells vs non-ADP/non-LS cells, $P = 0.070$; LS cells vs non-ADP/non-LS cells, $P = 0.15$, post hoc Tukey's multiple comparisons test) (Fig. 11B).

Optogenetic EPSCs in L1 cells from L5 CPn and Tlx3 cells

To examine innervation from L5 CPn and IT cells to L1 interneurons, ChR2 was introduced into Cre-expressing CPn or Tlx3 (IT) cells in M2 and activated by LED (Fig. 12A, left). Synaptic currents with multiple peaks were evoked in L1 cells by photostimulation of L5 PCs axons, especially those of Tlx3 cells (Fig. 12A 'Control'). To isolate monosynaptic EPSCs, TTX and 4-AP were added in the solution. Addition of TTX suppressed both spike induction at somata and EPSCs (Fig. 12A 'TTX'), but further inclusion of 4-AP again generated EPSCs (Fig. 12A 'TTX/4-AP') (Petreanu et al., 2009), assumed to be mediated by monosynaptic connections. In this condition, I observed EPSCs in all three classes of L1 cells by both CPn and Tlx3 cell axon stimulation (Fig. 12B). To examine innervation selectivity, two cells were simultaneously recorded and total charge of EPSC during 100 ms from stimulation onset (synaptic charge: SC) were compared (Fig. 13A). I found SC differences between two L1 cells of different classes, especially in the case of CPn cell stimulation (Fig. 13B). To compare the differences

quantitatively, I calculated the SC index in each pair of L1 cell classes: SCs difference divided by SCs sum. If the SC index were close to +1 or to -1, L5 PC input would be much stronger in one of the two L1 cells.

In CPn cell stimulation, LS cells had larger SCs than ADP cells (SC index = 0.71 ± 0.36, 6 pairs, $P = 0.0045$, one sample t test, hypothetical value = 0); non-ADP/non-LS cells had larger SCs than ADP cells (SC index = 0.44 ± 0.34, 13 pairs, $P = 0.0006$); and non-ADP/non-LS cells had larger SCs than LS cells (SC index = 0.53 ± 0.32, 6 pairs, $P = 0.0097$) (Fig. 13C 'CPn').

In Tlx3 stimulation, on the other hand, SCs were not different for all possible comparisons within the three classes: SC index = 0.05 ± 0.47 in LS cells vs. ADP cells, 5 pairs, $P = 0.81$; SC index = 0.04 ± 0.48 in non-ADP/non-LS cells vs. LS cells, 11 pairs, $P = 0.64$; SC index = -0.08 ± 0.37 in non-ADP/non-LS cells vs. LS cells, 6 pairs, $P = 0.56$; Fig. 13C 'Tlx3'). In each pair of postsynaptic L1 cell classes, CPn cell stimulation induced more biased input to a pair of cells than Tlx3 cell stimulation ($P = 0.026$ for LS vs. ADP cells; $P = 0.041$ for non-ADP/non-LS cells vs. LS cells and $P = 0.026$ for non-ADP/non-LS cells vs. LS cells, Mann Whitney test; Fig. 13C '#'). These results suggest that L5 Tlx3 cells can drive diverse L1 GABA cells more equally than CPn cells, while CPn inputs to L1 cells increase in strength with the following order to L1 cells as follows: ADP, LS and non-ADP/non-LS cells.

Discussion

The questions addressed in this study were whether L1 innervation from L5 in the frontal cortex, an important part of the top-down projection, was heterogeneous among and within PC subtypes; and whether L5 PC monosynaptic excitatory differed between postsynaptic L1 cell subtypes. I found L1 innervation heterogeneity among L5a PCs: CPn cells innervate upper L1 of proximal cortical areas; ER81 positive IT cells with higher L1 innervation preference project to both proximal and distal areas (Fig. 14 broad IT cells), whereas the other IT cells with lower L1 preference project only to the proximal areas (Fig. 14 restricted IT cells). Thus, M2-L5 sends three classes of outputs to M1 and S1, but only one class to the distal areas (Hirai et al., 2012; Ueta et al., 2013). I also found that excitations by L5 IT cells are generally similar between three L1 GABA cell subtypes, but that by CPn cells differs depending on the postsynaptic L1 GABA cell subtype (Fig. 14 right). CPn cells induced stronger excitation in the L1 cell subtype that innervates the upper L1 where the thalamocortical and CPn cell axons co-localize.

L5 IT cell diversity related to L1 innervation preference

ER81 was more expressed in broad IT cells than restricted IT cells. In L5 of mouse M1, IT cells expressing another transcription factor Fez family zinc finger 2 (Fezf2) differ in their intrinsic physiological characteristics and dendritic morphology from those that are negative for Fezf2 (Tantirigama et al., 2014). Fezf2-positive IT cells are distributed in L5a, but Fezf2-negative cells are more distributed in L5b, similar to ER81-positive and -negative IT cells (Fig. 5C) (Tantirigama et al., 2016). In rodent motor-related areas, IT cells that project to the distal areas such as visual, perirhinal and posterior parietal cortex are distributed in L5a, whereas L5b IT cells only project to in nearby areas

(Fig. 4B) (Ueta et al., 2013; Ueta et al., 2014). Since L5 the IT Fezf2 subtype in anterior lateral motor cortex does not necessarily express ER81 (Tasic et al., 2018), Fezf2-positive cells may partially overlap with ER81-positive broad IT cells.

In M2-L5, IT cells have diverse dendritic morphologies and innervate CPn cells unidirectionally; connected IT cell pairs exhibit similar dendritic morphologies (Morishima and Kawaguchi, 2006). L1 innervation of IT cells correlates with their dendritic length (Fig. 9A). Furthermore, firing pattern diversity in IT cells depends on their target cortical areas; connected IT cells exhibit similar firing patterns (Otsuka and Kawaguchi, 2008, 2011; Ueta et al., 2013). These results suggest more frequent synapse formation between IT cell subgroups sharing the target cortical area and layer. I consider that there are two types of local hierarchical connections to L5 CPn cells from broad and restricted IT cells, respectively (Fig. 14 gray arrows).

M2-L5 IT cells distributed axons in L1 and L2/3 of M1 more diffusely than the CPn cells with selective innervation to upper L1 (Fig. 3). L5 IT cells induce dendritic excitation in L2/3 PCs via the ascending axon collaterals towards L1 (Hirai et al., 2012). The circuit hierarchy in L5 suggests that output of L5 IT cells precedes that of CPn cells in the corticocortical projection. Therefore, M2-IT cells may participate in initial depolarization in M1-L2/3 cells and fire some of them. Next, at the distal apical dendritic tuft, the back-propagated spikes from previous firing could combine with the synaptic inputs from M2 CPn cells excited later than M2 IT cells. The conjunction of the two inputs would result in stronger depolarization in the distal dendritic tufts of M1 PCs, leading to synaptic potentiation by the top-down input (Larkum, 2013a)

Because broad and restricted IT cells differ in axon distribution in L1 and L2/3, they may excite different PCs in M1 as well as in M2 locally. This suggests that the two

groups of L5 IT cells in the frontal cortex make independent subnetworks not only in the local area but also in the target area of the top-down projection, and cooperate with the other top-down projection from CPn cells.

L1 inhibitory circuit activated by L5 CPn cells

L1 cells induce distinct effects in the cortical circuits. L1 contains two classes of GABA cells that either exhibit more inhibitory or disinhibitory effects on PCs, respectively (Jiang et al., 2013; Larkum, 2013b). The overall effect of a top-down input to L1 is determined by the activation balance between the inhibition and disinhibition classes (Ibrahim et al., 2016). Therefore, it is important to distinguish descending cells (disinhibition class) from other L1 cells. It has been reported that the descending cells can be reliably identified by the occurrence of ADP and absence of LS properties, which have been selected from a number of physiological parameters by machine learning (Cadwell et al., 2016). I developed a quantitative standard for detecting ADP (amplitude measurement) and LS (depolarization slope). In this study, similar to the previous study, more non-ADP/non-LS cells were found than ADP cells and LS cells (Schuman et al., 2019). CPn cells altered excitatory intensity according to the subtype of postsynaptic L1 GABA cells, which also supports the validity of GABA cell classification into the three subtypes used in this study.

Because there were ER81-positive and -negative Tlx3 cells in L5 (Fig. 4C top), Tlx3 cells include both IT cells with preferential L1 innervation (broad cells) and with diffuse innervation in L1 and L2/3 (restricted cells). Innervation strengths from broad IT cells were not different between any combination pairs of the L1 subtypes. To further understand the top-down inhibition/disinhibition circuits, the synaptic target of restricted

IT cells should be elucidated in L2/3.

LS and non-ADP/non-LS cells correspond morphologically to eNGF and canopy cells, respectively, both of which are inhibition classes (Jiang et al., 2013; Schuman et al., 2019). Because CPn cells activate the L1 inhibition classes rather than the disinhibition class (descending cell), they suppress some of PCs and emphasize the activity of uninhibited PCs, which would be used to select PC outputs of the top-down projection.

CPn cells preferentially excite canopy cells that innervate upper L1. On the other hand, thalamocortical innervations from ventromedial nucleus to LS (eNGF) cells are stronger than those to other L1 cells in prefrontal cortex including M2 (Cruikshank et al., 2012). Thus, L1 axons from both CPn and thalamic cells may prefer the inhibition class of L1 cells as the postsynaptic target. The eNGF cells induce both $GABA_A$ and $GABA_B$ inhibition on PCs, but canopy cells induce only $GABA_A$ inhibition of, shorter duration (Schuman et al., 2019). These observations suggest that inhibition by CPn cells via canopy cells is spatially and temporally limited. Upper L1 receives axons from CPn and thalamic cells. L5 CPn cells project to the thalamic nuclei, and these nuclei in turn innervate the upper L1 of cortex. Therefore, canopy cells may induce short-term feedforward suppression of excitation to the apical tufts of pyramidal cells from the thalamus in the cortico-thalamo-cortical loop connection.

This study suggests that L5 corticocortical cell subtypes show different connection selectivity not only in the L5 local circuitry, but also in projections to L1, an important pathway of top-down function. To better understand the function of the L5 to L1 projection, it is necessary to compare the innervation of the L1 PC tufts between L5 PC subtypes.

References

Abs E, Poorthuis RB, Apelblat D, Muhammad K, Pardi MB, Enke L, Kushinsky D, Pu DL, Eizinger MF, Conzelmann KK, Spiegel I, Letzkus JJ (2018) Learning-Related Plasticity in Dendrite-Targeting Layer 1 Interneurons. Neuron 100:684-699 e686.

Arlotta P, Molyneaux BJ, Chen J, Inoue J, Kominami R, Macklis JD (2005) Neuronal subtype-specific genes that control corticospinal motor neuron development in vivo. Neuron 45:207-221.

Barbas H (2015) General cortical and special prefrontal connections: principles from structure to function. Annu Rev Neurosci 38:269-289.

Barbas H, Rempel-Clower N (1997) Cortical structure predicts the pattern of corticocortical connections. Cereb Cortex 7:635-646.

Bastos AM, Usrey WM, Adams RA, Mangun GR, Fries P, Friston KJ (2012) Canonical microcircuits for predictive coding. Neuron 76:695-711.

Cadwell CR, Palasantza A, Jiang X, Berens P, Deng Q, Yilmaz M, Reimer J, Shen S, Bethge M, Tolias KF, Sandberg R, Tolias AS (2016) Electrophysiological, transcriptomic and morphologic profiling of single neurons using Patch-seq. Nat Biotechnol 34:199-203.

Cruikshank SJ, Ahmed OJ, Stevens TR, Patrick SL, Gonzalez AN, Elmaleh M, Connors BW (2012) Thalamic control of layer 1 circuits in prefrontal cortex. J Neurosci 32:17813-17823.

D'Souza RD, Burkhalter A (2017) A Laminar Organization for Selective Cortico-Cortical Communication. Front Neuroanat 11:71.

Economo MN, Clack NG, Lavis LD, Gerfen CR, Svoboda K, Myers EW, Chandrashekar J (2016) A platform for brain-wide imaging and reconstruction of individual neurons. Elife 5:e10566.

Felleman DJ, Van Essen DC (1991) Distributed hierarchical processing in the primate cerebral cortex. Cereb Cortex 1:1-47.

Gerfen CR, Paletzki R, Heintz N (2013) GENSAT BAC cre-recombinase driver lines to study the functional organization of cerebral cortical and basal ganglia circuits. Neuron 80:1368-1383.

Harb K, Magrinelli E, Nicolas CS, Lukianets N, Frangeul L, Pietri M, Sun T, Sandoz G, Grammont F, Jabaudon D, Studer M, Alfano C (2016) Area-specific development of distinct projection neuron subclasses is regulated by postnatal epigenetic modifications. Elife 5:e09531.

Harwell CC, Parker PR, Gee SM, Okada A, McConnell SK, Kreitzer AC, Kriegstein AR (2012) Sonic hedgehog expression in corticofugal projection neurons directs cortical microcircuit formation. Neuron 73:1116-1126.

Hestrin S, Armstrong WE (1996) Morphology and physiology of cortical neurons in layer I. J

Neurosci 16:5290-5300.

Hirai Y, Morishima M, Karube F, Kawaguchi Y (2012) Specialized cortical subnetworks differentially connect frontal cortex to parahippocampal areas. J Neurosci 32:1898-1913.

Ibrahim LA, Mesik L, Ji XY, Fang Q, Li HF, Li YT, Zingg B, Zhang LI, Tao HW (2016) Cross-Modality Sharpening of Visual Cortical Processing through Layer-1-Mediated Inhibition and Disinhibition. Neuron 89:1031-1045.

Jiang X, Wang G, Lee AJ, Stornetta RL, Zhu JJ (2013) The organization of two new cortical interneuronal circuits. Nat Neurosci 16:210-218.

Kaneko R, Takatsuru Y, Morita A, Amano I, Haijima A, Imayoshi I, Tamamaki N, Koibuchi N, Watanabe M, Yanagawa Y (2018) Inhibitory neuron-specific Cre-dependent red fluorescent labeling using VGAT BAC-based transgenic mouse lines with identified transgene integration sites. J Comp Neurol 526:373-396.

Kawaguchi Y (2017) Pyramidal Cell Subtypes and Their Synaptic Connections in Layer 5 of Rat Frontal Cortex. Cereb Cortex 27:5755-5771.

Kiritani T, Wickersham IR, Seung HS, Shepherd GM (2012) Hierarchical connectivity and connection-specific dynamics in the corticospinal-corticostriatal microcircuit in mouse motor cortex. J Neurosci 32:4992-5001.

Kuan L, Li Y, Lau C, Feng D, Bernard A, Sunkin SM, Zeng H, Dang C, Hawrylycz M, Ng L (2015) Neuroinformatics of the Allen Mouse Brain Connectivity Atlas. Methods 73:4-17.

Lam YW, Sherman SM (2019) Convergent synaptic inputs to layer 1 cells of mouse cortex. Eur J Neurosci 49:1388-1399.

Larkum M (2013a) A cellular mechanism for cortical associations: an organizing principle for the cerebral cortex. Trends Neurosci 36:141-151.

Larkum ME (2013b) The yin and yang of cortical layer 1. Nat Neurosci 16:114-115.

Madisen L, Zwingman TA, Sunkin SM, Oh SW, Zariwala HA, Gu H, Ng LL, Palmiter RD, Hawrylycz MJ, Jones AR, Lein ES, Zeng H (2010) A robust and high-throughput Cre reporting and characterization system for the whole mouse brain. Nat Neurosci 13:133-140.

Makino H, Ren C, Liu H, Kim AN, Kondapaneni N, Liu X, Kuzum D, Komiyama T (2017) Transformation of Cortex-wide Emergent Properties during Motor Learning. Neuron 94:880-890 e888.

Manita S, Suzuki T, Homma C, Matsumoto T, Odagawa M, Yamada K, Ota K, Matsubara C, Inutsuka A, Sato M, Ohkura M, Yamanaka A, Yanagawa Y, Nakai J, Hayashi Y, Larkum ME, Murayama M (2015) A Top-Down Cortical Circuit for Accurate Sensory Perception. Neuron 86:1304-1316.

Markov NT, Vezoli J, Chameau P, Falchier A, Quilodran R, Huissoud C, Lamy C, Misery P, Giroud

P, Ullman S, Barone P, Dehay C, Knoblauch K, Kennedy H (2014) Anatomy of hierarchy: feedforward and feedback pathways in macaque visual cortex. J Comp Neurol 522:225-259.

Mejias JF, Murray JD, Kennedy H, Wang XJ (2016) Feedforward and feedback frequency-dependent interactions in a large-scale laminar network of the primate cortex. Sci Adv 2:e1601335.

Molyneaux BJ, Arlotta P, Fame RM, MacDonald JL, MacQuarrie KL, Macklis JD (2009) Novel subtype-specific genes identify distinct subpopulations of callosal projection neurons. J Neurosci 29:12343-12354.

Morishima M, Kawaguchi Y (2006) Recurrent connection patterns of corticostriatal pyramidal cells in frontal cortex. J Neurosci 26:4394-4405.

Morishima M, Morita K, Kubota Y, Kawaguchi Y (2011) Highly differentiated projection-specific cortical subnetworks. J Neurosci 31:10380-10391.

Morishima M, Kobayashi K, Kato S, Kawaguchi Y (2017) Segregated Excitatory-Inhibitory Recurrent Subnetworks in Layer 5 of the Rat Frontal Cortex. Cereb Cortex 27:5846-5857.

Morita K, Im S, Kawaguchi Y (2019) Differential Striatal Axonal Arborizations of the Intratelencephalic and Pyramidal-Tract Neurons: Analysis of the Data in the MouseLight Database. Front Neural Circuits 13:71.

Muralidhar S, Wang Y, Markram H (2013) Synaptic and cellular organization of layer 1 of the developing rat somatosensory cortex. Front Neuroanat 7:52.

Otsuka T, Kawaguchi Y (2008) Firing-pattern-dependent specificity of cortical excitatory feed-forward subnetworks. J Neurosci 28:11186-11195.

Otsuka T, Kawaguchi Y (2011) Cell diversity and connection specificity between callosal projection neurons in the frontal cortex. J Neurosci 31:3862-3870.

Palmer LM, Schulz JM, Murphy SC, Ledergerber D, Murayama M, Larkum ME (2012) The cellular basis of GABA(B)-mediated interhemispheric inhibition. Science 335:989-993.

Petreanu L, Mao T, Sternson SM, Svoboda K (2009) The subcellular organization of neocortical excitatory connections. Nature 457:1142-1145.

Rubio-Garrido P, Perez-de-Manzo F, Porrero C, Galazo MJ, Clasca F (2009) Thalamic input to distal apical dendrites in neocortical layer 1 is massive and highly convergent. Cereb Cortex 19:2380-2395.

Schuman B, Machold RP, Hashikawa Y, Fuzik J, Fishell GJ, Rudy B (2019) Four Unique Interneuron Populations Reside in Neocortical Layer 1. J Neurosci 39:125-139.

Shipp S (2005) The importance of being agranular: a comparative account of visual and motor cortex. Philos Trans R Soc Lond B Biol Sci 360:797-814.

Shipp S, Adams RA, Friston KJ (2013) Reflections on agranular architecture: predictive coding in

the motor cortex. Trends Neurosci 36:706-716.

Tantirigama ML, Oswald MJ, Duynstee C, Hughes SM, Empson RM (2014) Expression of the developmental transcription factor Fezf2 identifies a distinct subpopulation of layer 5 intratelencephalic-projection neurons in mature mouse motor cortex. J Neurosci 34:4303-4308.

Tantirigama ML, Oswald MJ, Clare AJ, Wicky HE, Day RC, Hughes SM, Empson RM (2016) Fezf2 expression in layer 5 projection neurons of mature mouse motor cortex. J Comp Neurol 524:829-845.

Tasic B et al. (2016) Adult mouse cortical cell taxonomy revealed by single cell transcriptomics. Nat Neurosci 19:335-346.

Tasic B et al. (2018) Shared and distinct transcriptomic cell types across neocortical areas. Nature 563:72-78.

Ueta Y, Hirai Y, Otsuka T, Kawaguchi Y (2013) Direction- and distance-dependent interareal connectivity of pyramidal cell subpopulations in the rat frontal cortex. Front Neural Circuits 7:164.

Ueta Y, Otsuka T, Morishima M, Ushimaru M, Kawaguchi Y (2014) Multiple layer 5 pyramidal cell subtypes relay cortical feedback from secondary to primary motor areas in rats. Cereb Cortex 24:2362-2376.

Winnubst J et al. (2019) Reconstruction of 1,000 Projection Neurons Reveals New Cell Types and Organization of Long-Range Connectivity in the Mouse Brain. Cell 179:268-281 e213.

Wozny C, Williams SR (2011) Specificity of synaptic connectivity between layer 1 inhibitory interneurons and layer 2/3 pyramidal neurons in the rat neocortex. Cereb Cortex 21:1818-1826.

Yeterian EH, Pandya DN, Tomaiuolo F, Petrides M (2012) The cortical connectivity of the prefrontal cortex in the monkey brain. Cortex 48:58-81.

Yoneshima H, Yamasaki S, Voelker CC, Molnar Z, Christophe E, Audinat E, Takemoto M, Nishiwaki M, Tsuji S, Fujita I, Yamamoto N (2006) Er81 is expressed in a subpopulation of layer 5 neurons in rodent and primate neocortices. Neuroscience 137:401-412.

Table 1. Coordinates of tracer and virus injection sites

Region	Coordinates (mm)			Tracer, virus
	Rostrocaudal (From bregma)	Mediolateral (From midline)	Dorsoventral (From pia)	
M1	1.5	2.0	0.1 - 0.7	CTB-647, FB
S1	0	2.2	0.1 - 0.9	CTB-647, RetroBeads, FB
	0	3.5	0.1 - 1.2	
PRC	-1.6	5.7[§]	0.3 - 1.0	CTB-647
	-1.8	5.7[§]	0.3 - 1.0	
Vis	-3.0	2.5	0.1 - 0.6	CTB-647, RetroBeads
	-4.0	2.5	0.1 - 0.6	
Pons	-4.2	0.6	5.8 - 6.2	CTB-647, AAV 2.retro pgk-Cre
M2 (Axon labeling)	1.5	0.7	0.7 - 0.9	AAV2.5 Synaptophysin-EGFP
M2	2.0	1.0	0.7 - 0.9	AAV2.5h ChR2(H134R)-mCherry
(ChR2)	1.2	0.6	0.7 - 0.9	

Cortical areas: M1, primary motor cortex; S1, primary somatosensory cortex; PRC, perirhinal cortex; Vis, visual cortex; M2, secondary motor cortex.

Tracers: CTB-647, Alexa Fluor 647-conjugated cholera toxin subunit B; RetroBeads, red fluorescent RetroBeads ; FB, Fast Blue.

Viruses: AAV2.5 Synaptophysin-EGFP, AAV 2.5 CAG Double flox Synaptophysin-EGFP WPRE; AAV2.5 hChR2(H134R)-mCherry, AAV 2.5 pAAV-EF1a-double floxed-hChR2(H134R)-mCherry-WPRE-HGHpA.

[§], injection pipette positioned at a 30° lateral inclination.

Table 2. List of ID and DOI of each neuron data in MouseLight.

ID	DOI	ID	DOI
For axon analysis			
M2-L5 CPn			
AA0011	10.25378/janelia.5521615	AA0245	10.25378/janelia.5527657
AA0250	10.25378/janelia.5527678	AA0415	10.25378/janelia.7614212
AA0764	10.25378/janelia.7710065		
M2-L5 IT (commissural cell)			
AA0190	10.25378/janelia.5527474	AA0230	10.25378/janelia.5527603
AA0233	10.25378/janelia.5527612	AA0236	10.25378/janelia.5527621
AA0265	10.25378/janelia.5527738	AA0269	10.25378/janelia.5527753
AA0274	10.25378/janelia.5527774	AA0324	10.25378/janelia.7613486
AA0332	10.25378/janelia.7613684	AA0397	10.25378/janelia.7614113
AA0400	10.25378/janelia.7614122	AA0411	10.25378/janelia.7614194
AA0412	10.25378/janelia.7614200	AA0421	10.25378/janelia.7614233
AA0422	10.25378/janelia.7614236	AA0441	10.25378/janelia.7614356
AA0445	10.25378/janelia.7614596	AA0460	10.25378/janelia.7615835
AA0465	10.25378/janelia.7615889	AA0466	10.25378/janelia.7615895
AA0473	10.25378/janelia.7615961	AA0534	10.25378/janelia.7640063
AA0575	10.25378/janelia.7649846	AA0632	10.25378/janelia.7658054
AA0646	10.25378/janelia.7658126	AA0734	10.25378/janelia.7707296
AA0735	10.25378/janelia.7707302	AA0746	10.25378/janelia.7707365
AA0749	10.25378/janelia.7707374	AA0767	10.25378/janelia.7710077
AA0798	10.25378/janelia.7739537	AA0840	10.25378/janelia.7739903
AA0841	10.25378/janelia.7739909	AA0842	10.25378/janelia.7739915
AA0853	10.25378/janelia.7739954	AA0887	10.25378/janelia.7742807
AA0905	10.25378/janelia.7780856		
Axonal length in L1/2/3 less than 1308 µm			
M2-L5 CPn			
AA0115	10.25378/janelia.5526724	AA0122	10.25378/janelia.5527240
AA0181	10.25378/janelia.5527444	AA0182	10.25378/janelia.5527447
AA0576	10.25378/janelia.7649849	AA0726	10.25378/janelia.7707194
AA0780	10.25378/janelia.7739285	AA0788	10.25378/janelia.7739369
AA0791	10.25378/janelia.7739399	AA0792	10.25378/janelia.7739402
AA0882	10.25378/janelia.7742783		

ID	DOI	ID	DOI
M2-L5 IT			
AA0279	10.25378/janelia.5527792	AA0281	10.25378/janelia.5527798
M2-L5 neither CPn nor IT			
AA0235	10.25378/janelia.5527618	AA0286	10.25378/janelia.5527813
AA0300	10.25378/janelia.5527855	AA0462	10.25378/janelia.7615862
AA0556	10.25378/janelia.7640234	AA0602	10.25378/janelia.7650038
AA0786	10.25378/janelia.7739330	AA0787	10.25378/janelia.7739366
AA0797	10.25378/janelia.7739534	AA0846	10.25378/janelia.7739927
AA0867	10.25378/janelia.7740095	AA0874	10.25378/janelia.7742570
AA0888	10.25378/janelia.7742810	AA0907	10.25378/janelia.7780862
M2-L5 in MouseLight but not in Allen atlas			
AA0012	10.25378/janelia.5521618	AA0059	10.25378/janelia.5521780
AA0179	10.25378/janelia.5527438	AA0180	10.25378/janelia.5527441
AA0267	10.25378/janelia.5527747	AA0285	10.25378/janelia.5527810
AA0452	10.25378/janelia.7615274	AA0481	10.25378/janelia.7615991
AA0583	10.25378/janelia.7649900	AA0858	10.25378/janelia.7740017

Table 3 Electrophysiological properties of L1 GABA cells.

	(a) ADP cell (n = 38)	(b) LS cell (n = 13)	(c) non-ADP/ non-LS cell (n = 45)	Kruskal-Wallis test,
Resting potential (mV)	-61.3 ± 5.4	-63.8 ± 6.9	-62.2 ± 7.8	$P = 0.53$
Input resistance (MΩ)	206 ± 102	221 ± 57	195 ± 143	$P = 0.11$
Time constant (ms)	10.5 ± 5.2	12.3 ± 4.3	10.0 ± 5.3	$P = 0.12$
F/I slope (Hz/nA)	46.7 ± 30.3	67.5 ± 16.5	61.4 ± 42.7	$P = 0.072$

Data, mean ± SD.

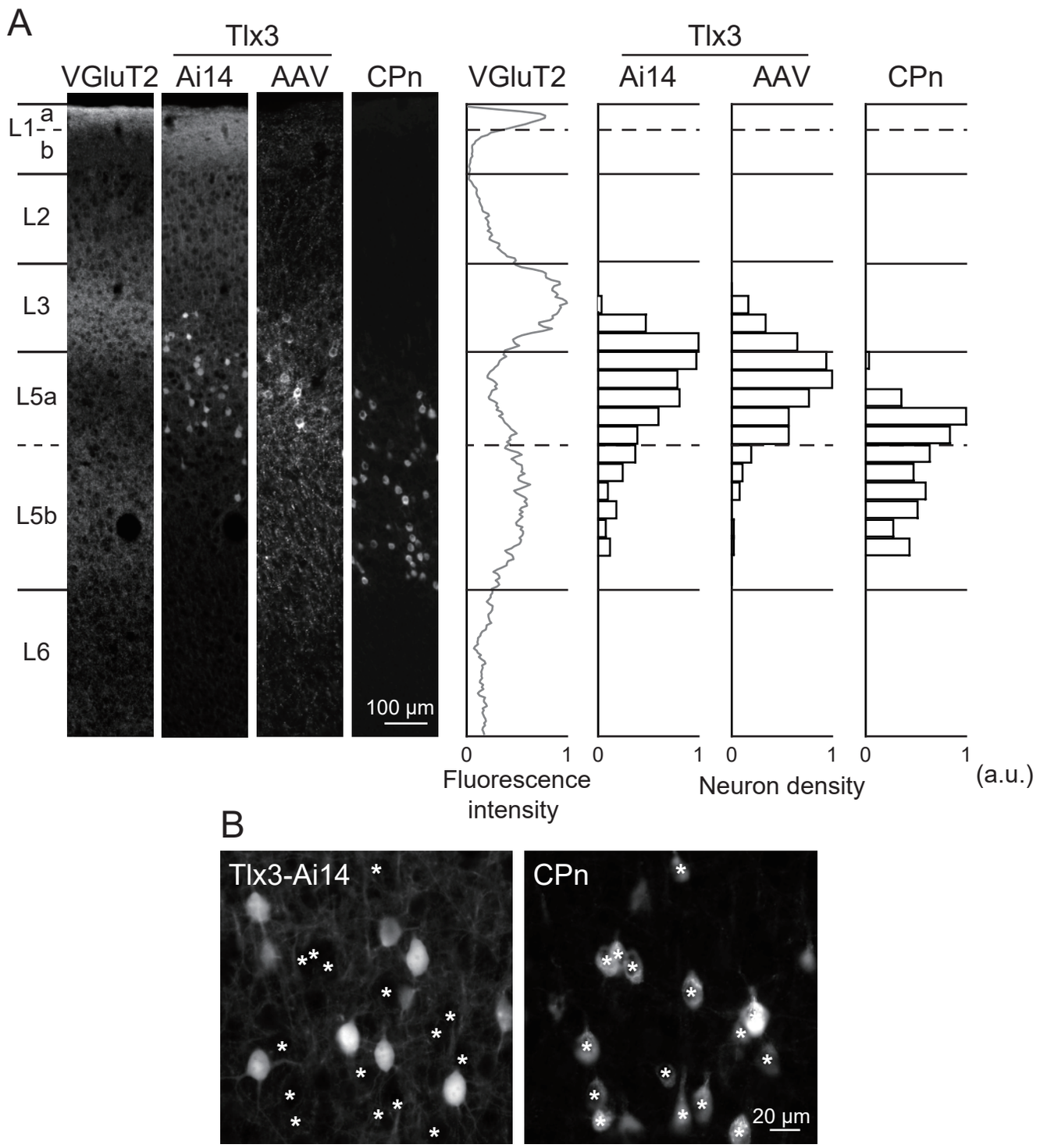

Figure 1. Laminar distributions of Cre-expressing cells in Tlx3 mouse line.

A: Laminar distributions of Tlx3 and CPn cells. Cre expression in Tlx3 cells was detected by crossing with the reporter line (Ai14) or local injection of AAV into M2. CPn cells were labeled with a retrograde tracer (CTB-647). Layers were identified with cell density and VGluT2 immunoreactivity. Sections shown in the left: 0.2 mm wide and 20-μm-thick. In the right, the laminar profile of VGluT2 immunoreactivity was quantified by fluorescence intensity at depth intervals of 5 μm. The fluorescently labeled somata were counted at depth intervals of one-fifth of L5a thickness.

B: Tlx3 cells independent of CPn cells. CPn cells labeled by a retrograde tracer were not overlapped with Tlx3 cells (asterisk).

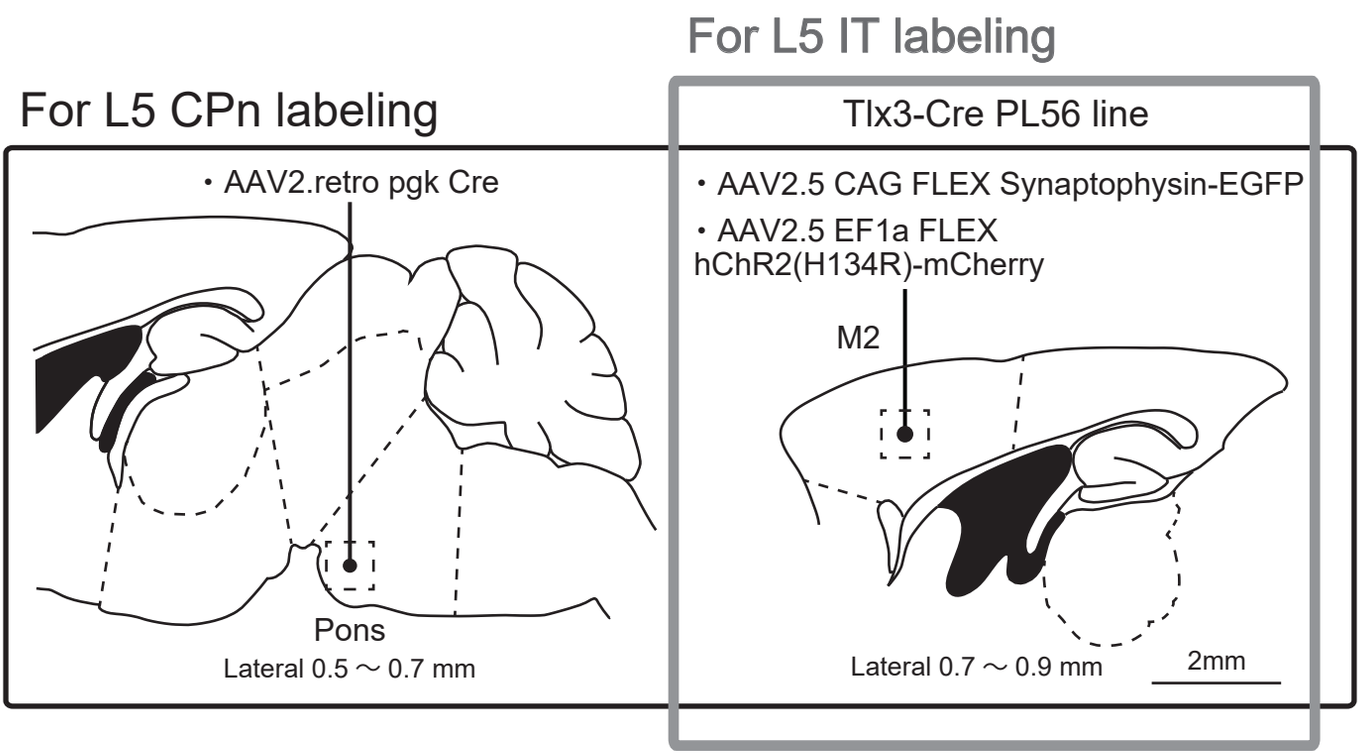

Figure 2. Selective fluorescence or ChR2 labeling of CPn and Tlx3 cells by virus injections. Cre was loaded in CPn cells by retrograde virus injection into the pons (Cre-CPn cells). The fluorescent protein/ChR2 was expressed by local M2 injection of another virus with Cre-dependent expression of them in the Cre-CPn or Tlx3 cells. Reference atlas: The Mouse Brain in Stereotaxic Coordinates (George Paxinos and Keith B. J. Franklin, 2001)

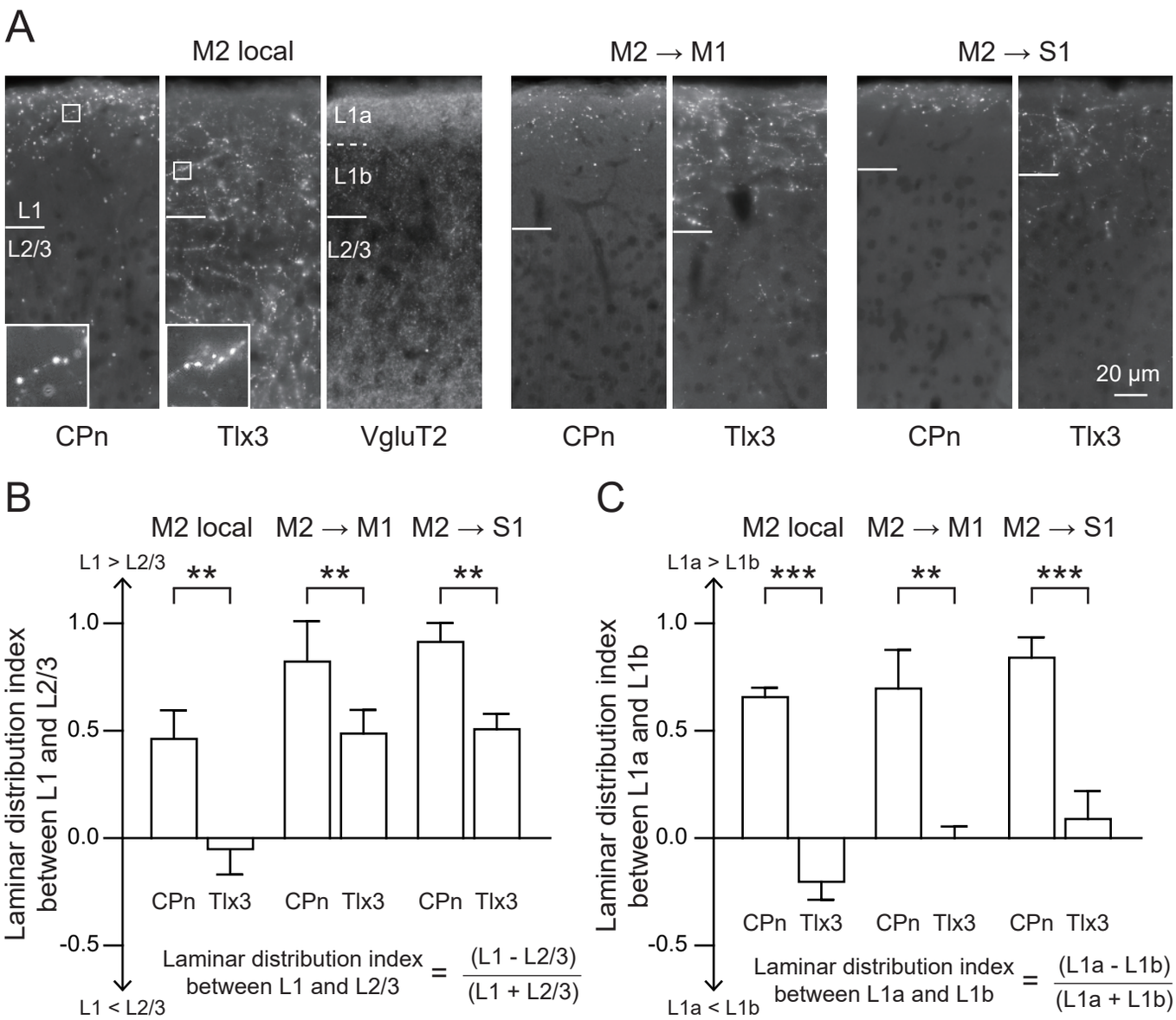

Figure 3. Axon distributions of M2 CPn and Tlx3 cells in L1 and L2/3 of M2 local, M1 and S1.

A: Axonal distributions in M2 local (left) and ipsilateral M1 (right). Axon fibers were labeled by Cre-dependent induction of Synaptophysin-EGFP, which accumulated preferentially in the axon terminals (seen as puncta in the photograph).

B: Distribution differences of fluorescent puncta originatinged from M2-L5 PCs between L1 and L2/3 in M2 local, M1 and S1. The difference was quantified by laminar distribution index of punctaum density: positive for L1 preference and negative for L2/3 preference. Data, mean + SD (n = 3 for each). $^{**}P < 0.01$ (unpaired t test)

C: Distribution differences of fluorescent puncta between L1a and L1b. L1a stronger VGluT2 immunoreactivity than L1b (A).$^{**}P < 0.001$, $^{***}P < 0.001$ (unpaired t test).

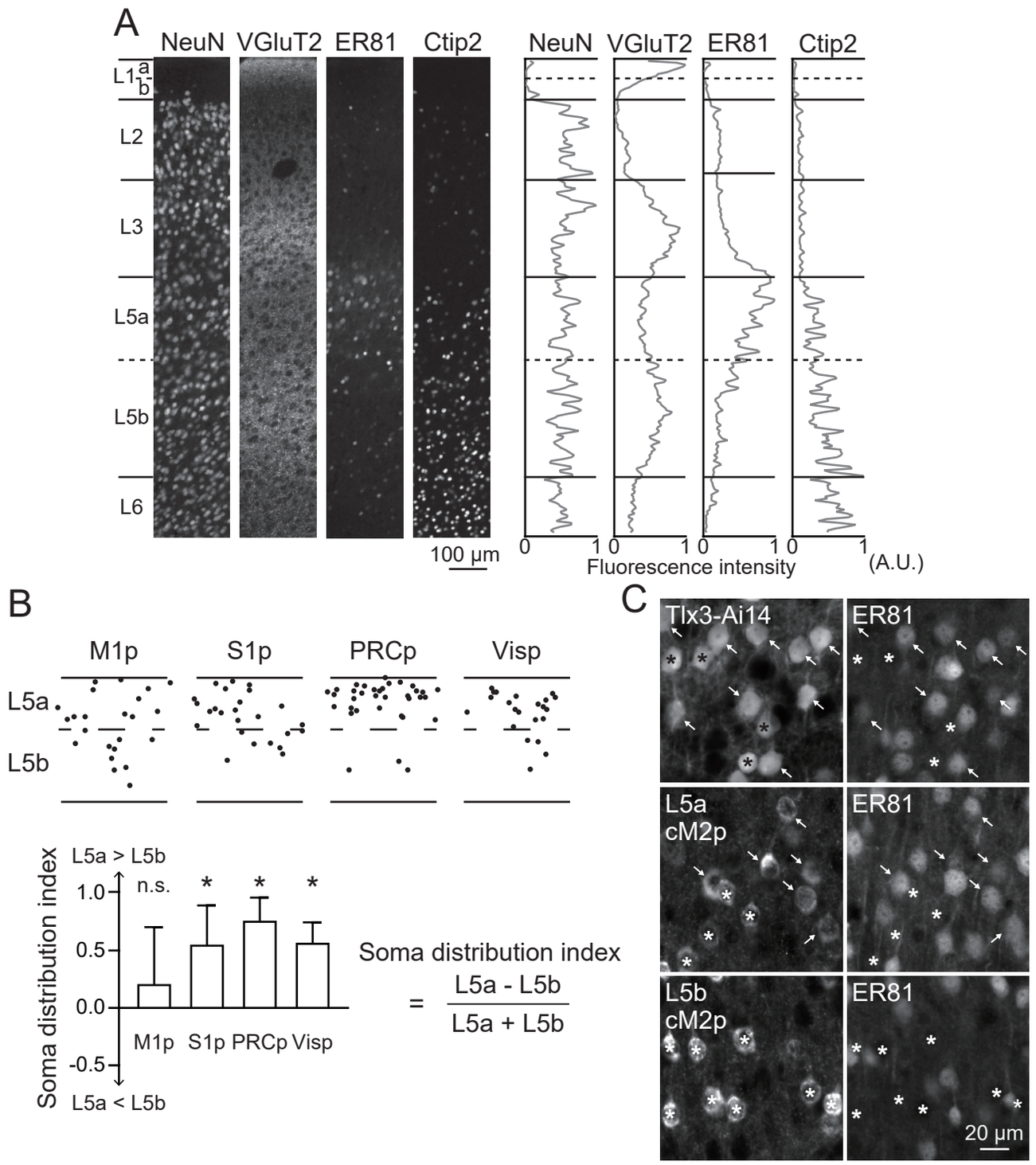

Figure 4. ER81 expression in a subpopulation of IT cells in L5a, but not in L5b

A：Laminar distribution of ER81- and Ctip2-positive neurons. The layers were identified by immunofluorescence for NeuN and VGluT2. Sections: 0.2 mm wide and 20-μm-thick. Fluorescence intensities of area was quantified at row widths of 5 μm were normalized by the maximum value.

B: Corticocortical cells were present in L5a more than in L5b. Laminar distributions of M2-L5 cells labeled retrogradely from other areas. Data are mean + SD. $*P < 0.05$ (one sample t test, hypothetical value = 0). M1p, primary motor cortex projecting; S1, primary somatosensory cortex projecting; PRC, perirhinal cortex projecting; Vis, visual cortex projecting.

C: ER81-positive and -negative IT cells in L5a. Top, Tlx3 cells positive (arrows) and negative (asterisks) for ER81. Middle and bottom, contralateral M2 projecting (cM2p)-cells were positive (arrows) and negative for ER81cells (asterisks) in L5a, but mostly negative for ER81 in L5b.

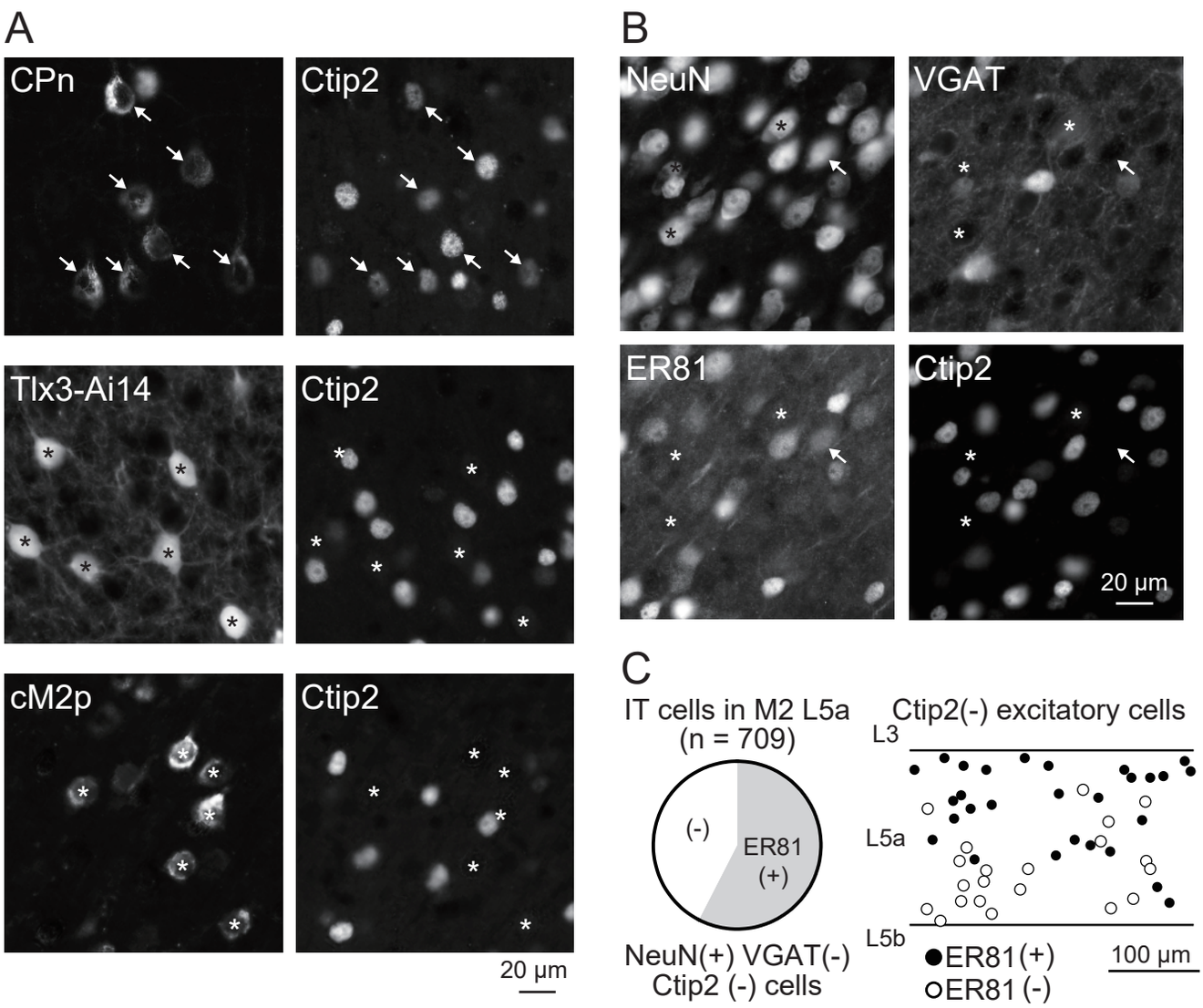

Figure 5. Ratio of ER81-expressing cells among M2-L5a IT cells

A: Ctip2 expression in L5a CPn cells, but not in L5a IT cells. Ctip2 was expressed in almost all CPn cells (arrows in top), but not expressed in Tlx3 cells (asterisks in middle) and in cM2p cells in L5a (asterisks in bottom). In L5b, on the other hand some cM2p cells expressed Ctip2 (not shown).

B: ER81 expression heterogeneity in L5a IT cells. L5a IT cells were identified by NeuN expression without VGAT-tdTomato and Ctip2 expression. Arrow, ER81-positive IT cells; asterisks, ER81-negative IT cells.

C: Ratio and distribution of ER81-positive and -negative IT cells in M2-L5a.

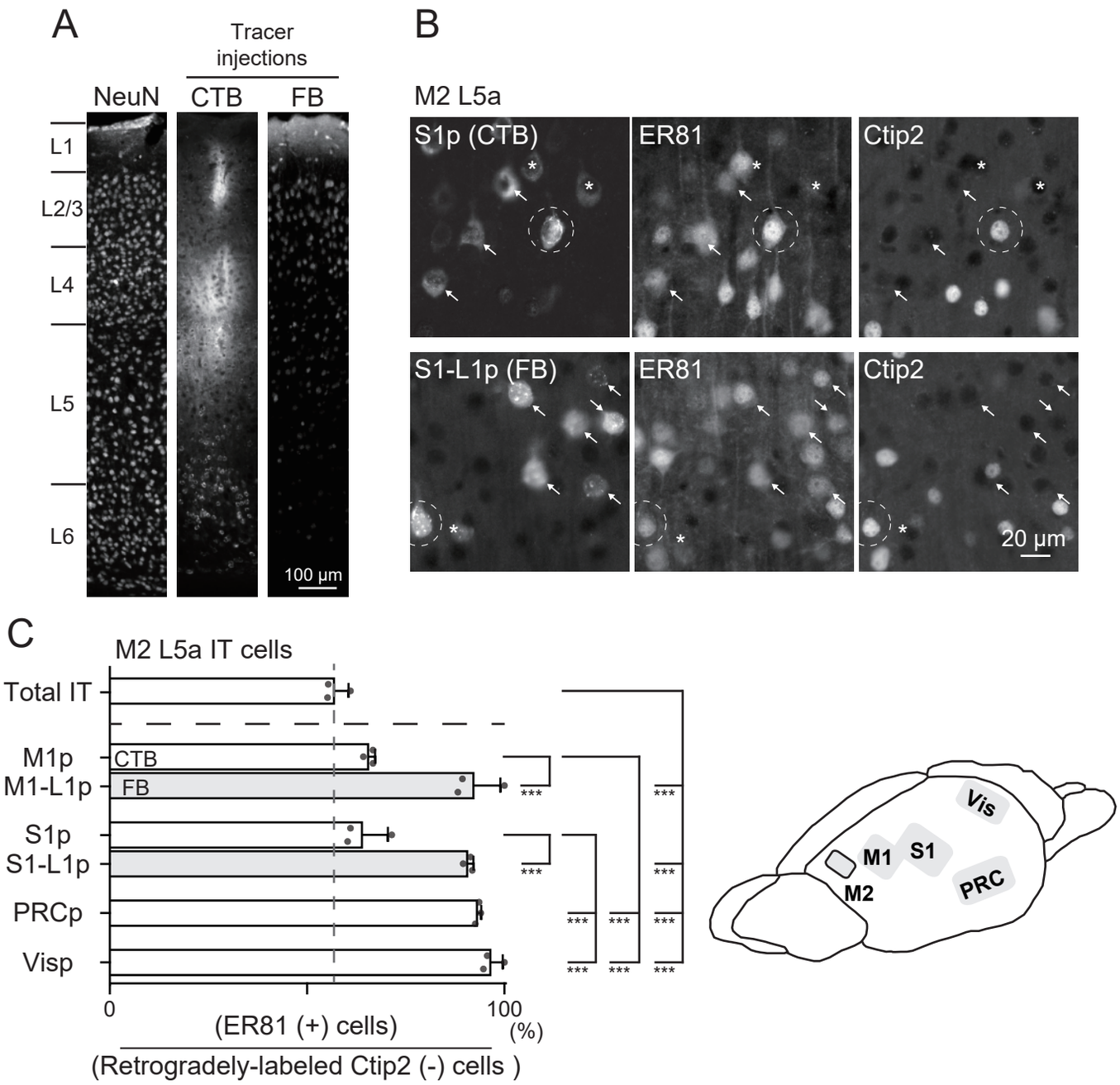

Figure 6. ER81 expression in M2-L5a related to L1 innervation and distal cortex projection.

A: Two kinds of retrograde labeling: CTB injection into deep layers and FB application onto the cortical surface (L1p: L1-projecting). In CTB, three images were overlaid.

B: ER81 expression in S1-projecting (S1p) cells (top) and S1-L1p cells (bottom). S1p cells were positive (arrows) or negative (asterisks) for ER81, but S1-L1p cells were mostly positive for ER81 (arrows). Some S1p and S1-L1p cells were positive for Ctip2 (dashed circle).

C: Proportion of ER81 cells in corticocortical L5a IT cells. The proportion was higher in corticocortical cells projecting to the PRC and Vis cortices than those to M1 and S1; and higher in M1-L1p and S1-L1p cells than M1p and S1p cells, respectively (n = 3 for each). ***$P < 0.001$ (ordinary one-way ANOVA, $P < 0.0001$; post hoc Tukey's multiple comparisons test). Inset, M2 and areas where tracers were injected.

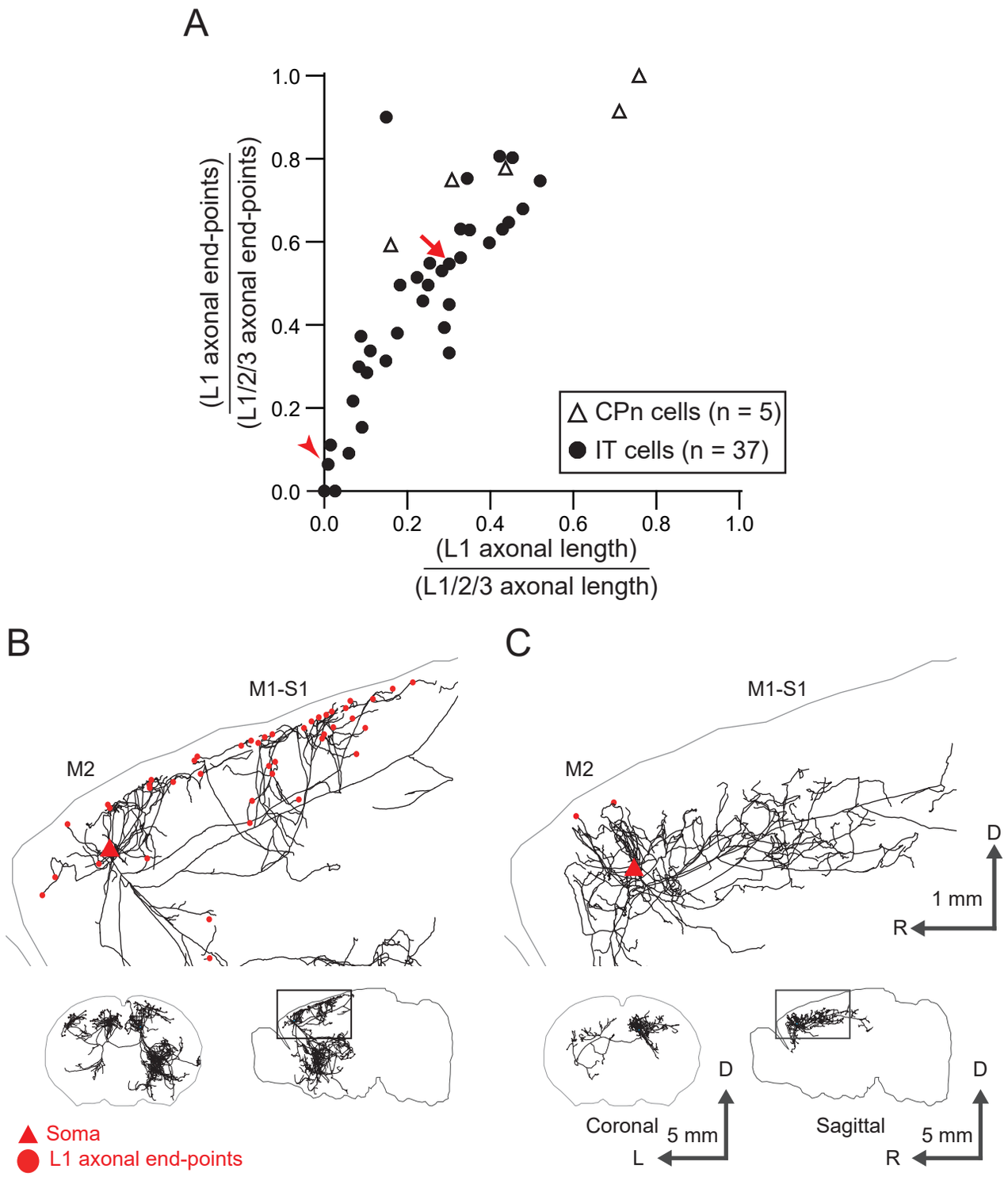

Figure 7. L1 innervation heterogeneity of M2-L5 CPn and IT cells obtained from the MouseLight database of Janelia Research Campus.

A: L1 distribution ratios of axonal length and end-points in axons innervating L1 and L1/2/3. Those were both diverse and well correlated.

B: L5 IT cell with extending axons and many end-points (red circles) in L1. This cell corresponds to arrow in (A). Red triangle, Soma.

C: L5 IT cell with few axons and end-points in L1. This cell corresponds to arrowhead in (A).

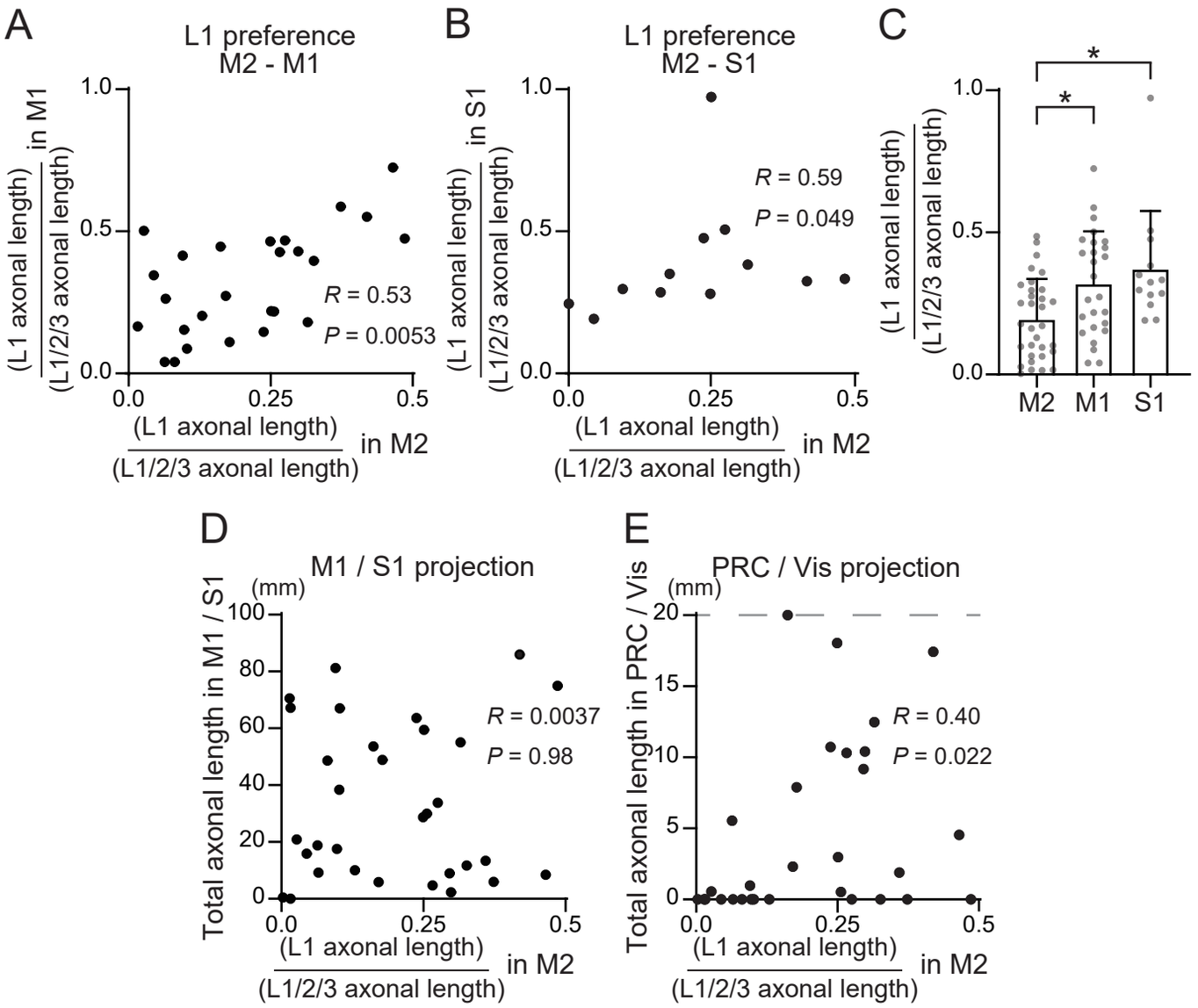

Figure 8. L1-inervation preferences common among the target areas and correlated with distal projection.

A,B: Relationship between L1 proportions of axonal length in M1 and in M2 (A) and those in S1 and in M2 (B).Cells innervating L1 were analyzed. *R* and *P*, Spearman correlation test.

C: L1 proportions of axonal length in M2, M1 and S1. $P = 0.0036$, Kruskal-Wallis test. $^*P < 0.05$, post hoc Dunn's multiple comparisons test.

D,E: Relation of the total axon length in target areas to L1 length proportion in M2. These were not correlated using M1 and S1 as target cortical areas (D), but positively correlated using perirhinal and visual cortices as targets (E). Axon length longer than 20 mm was plotted on 20 mm in (E).

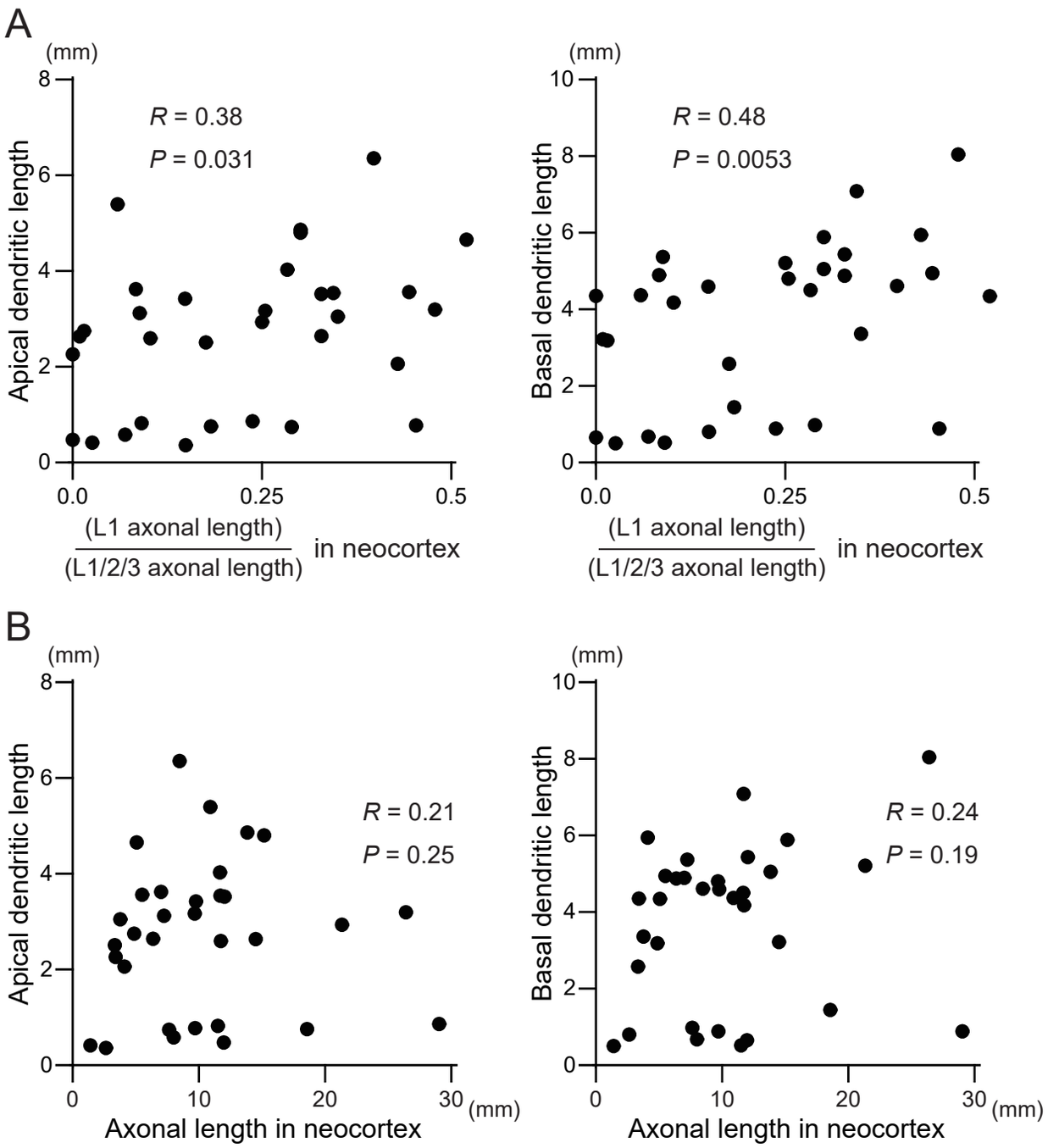

Figure 9. Relation of dendritic morphologies with the L1 innervation preference.

A: Relation of dendritic length with L1 axonal length proportions. Left, apical dendrites; right, basal dendrites. *R* and *P*, Spearman correlation test.

B: Relation of dendritic length with total axonal length in neocortex. Left, apical dendrites; right, basal dendrites.

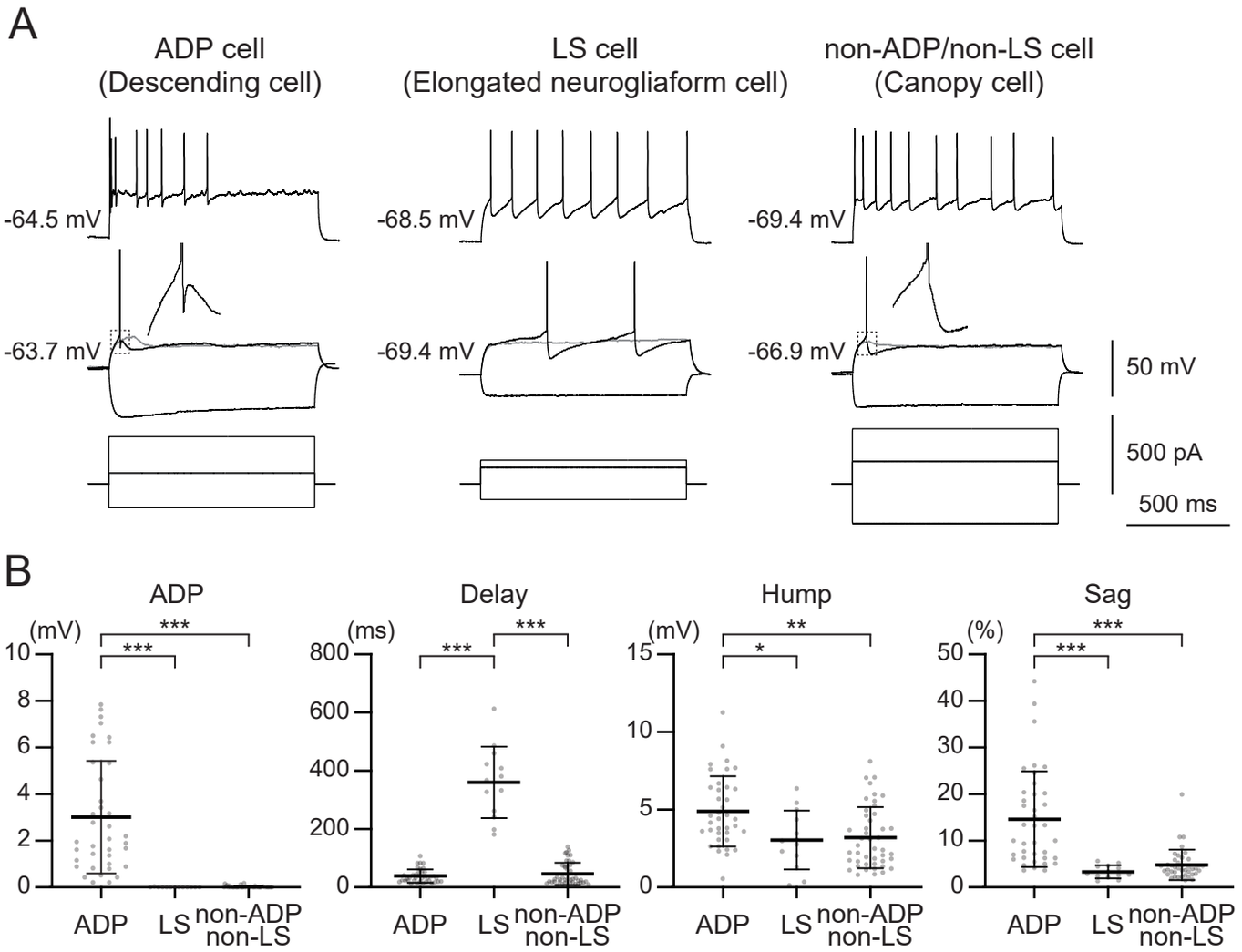

Figure 10. Electrophysiological classification of L1 cells in M2

A: Three classes of L1 cells: ADP, LS and non-ADP/non-LS cells, identified by depolarizing and firing responses to current pulses. ADP, afterdepolarization; LS, late spiking.

B: Intrinsic electrophysiological properties of the L1 cell subtypes: ADP amplitude, (ADP), delay time to the initial spike just at the threshold (Delay), amplitude of depolarizing hump just below the threshold stimulation (Hump), and hyperpolarizing sag proportion (Sag). Kruskal-Wallis test. *$P < 0.05$, **$P < 0.01$, ***$P < 0.001$, post hoc Dunn's multiple comparisons test.

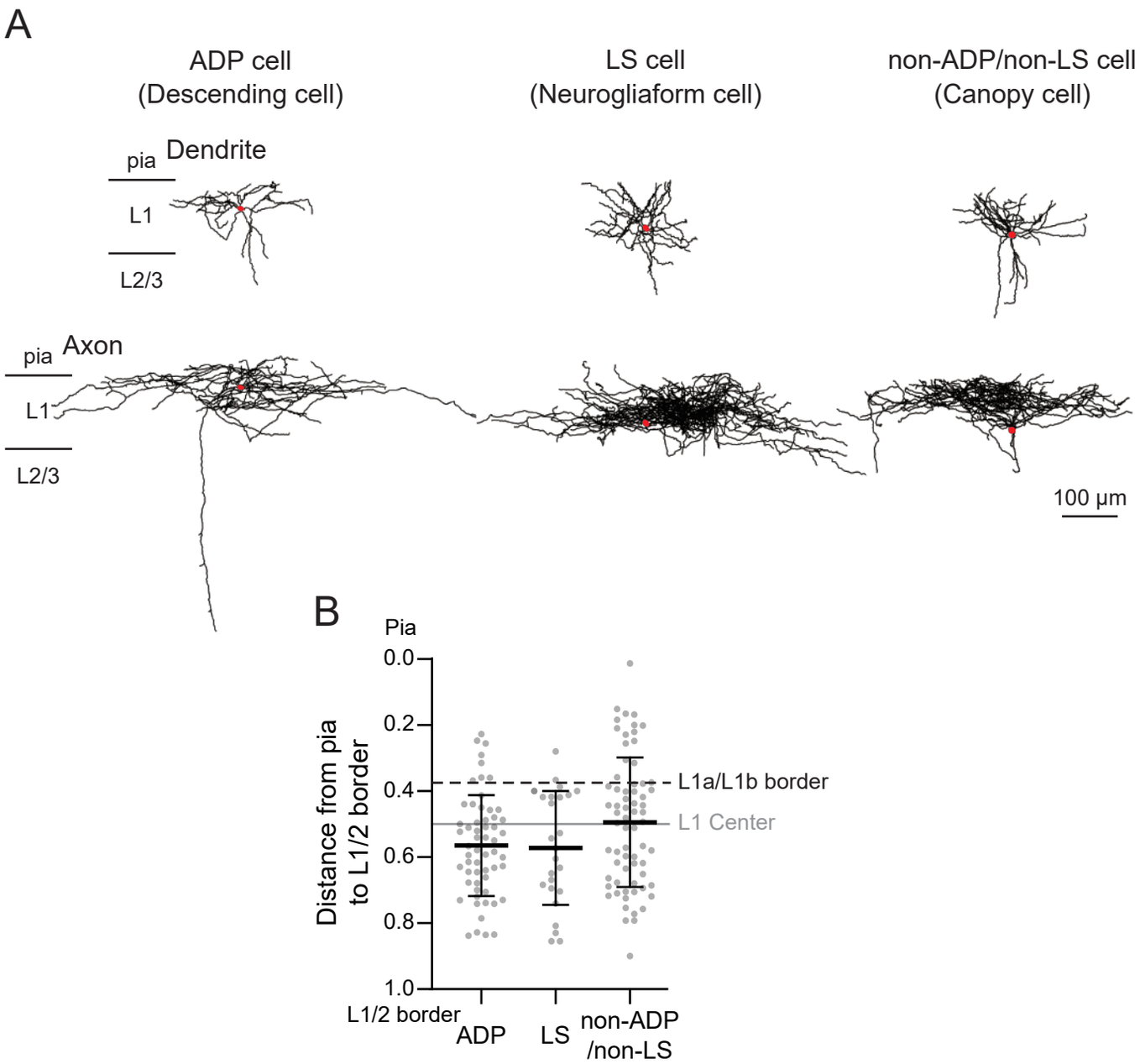

Figure 11. Dendrite and axon reconstructions of L1 cells identified physiologically.

A: Reconstructions of three cells of different physiological subtypes. Upper, somata (red) and dendrites (black); lower, somata (red) and axons (black).

B: Soma distribution along the L1 depth (0, pia; 1.0, L1/2 border). A dashed line is border of L1a/L1b and a gray line is half of L1 depth (0.5). ordinary one-way ANOVA (P = 0.045) and post hoc Tukey's multiple comparisons test ($P > 0.05$).

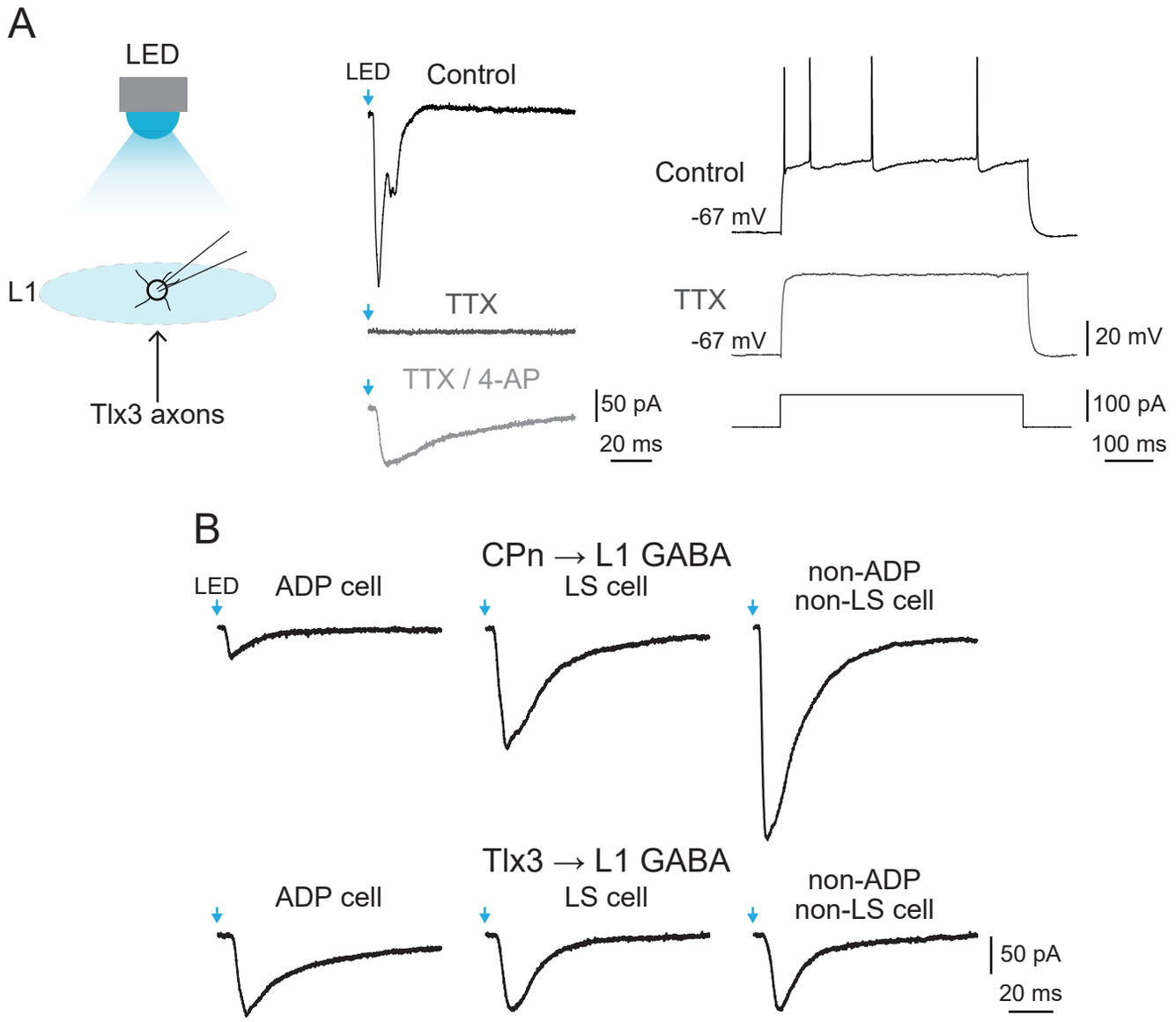

Figure 12. Photostimulation of L1 axons from L5 PCs

A: EPSC induction by photostimulation of Tlx3 cells axons. The EPSC and spike firing were blocked by TTX (0.5 μM) application shown in the center and right columns, respectively. Addition of 4-AP (1 mM) reproduced EPSCs in L1 cells (center column). Blue rrow, photostimulation (duration, 1 ms).

B: EPSCs induced in L1 cell subtypes by photostimulation of CPn and Tlx3 cell axons in the solution containing TTX and 4-AP.

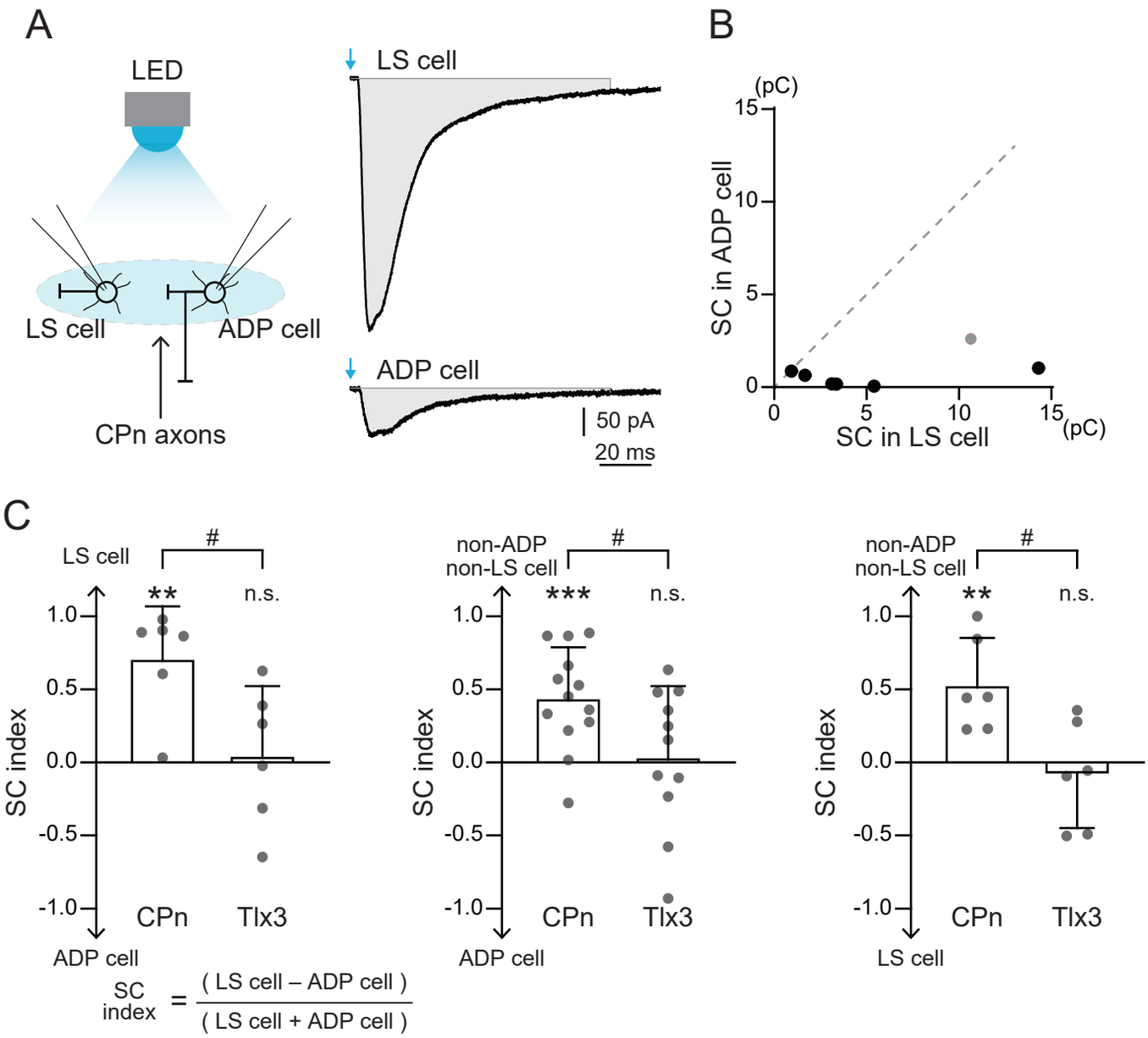

Figure 13. EPSC induction dependent on the presynaptic L5 and postsynaptic L1 cell subtypes.

A: Photo-induced EPSCs recorded from two L1 cells of different classes (LS and ADP cells in this case). The recording solution contained TTX and 4-AP. Gray area, inward current charge during 100 ms from the stimulation onset (blue arrow), used for estimation of synaptic strength (SC: synaptic charge).

B: Relation of CPn cell axon-induced SCs between LS and ADP cells, recorded simultaneously. Gray circle, a cell pair shown in (A).

C: Input strength comparison between two postsynaptic L1 subtypes, using SC index: [(SC in cell 1) - (SC in cell 2)] / [(SC in cell 1) + (SC in cell 2)]. The input bias between two postsynaptic cells from a presynaptic L5 PC subtype was tested by onw sample t test (hypothetical value = 0; $^{**}P < 0.01$, $^{***}P < 0.001$). The bias difference between presynaptic CPn and Tlx3 cells was tested by Mann Whitney test ($\#P < 0.05$). Data are mean + SD.

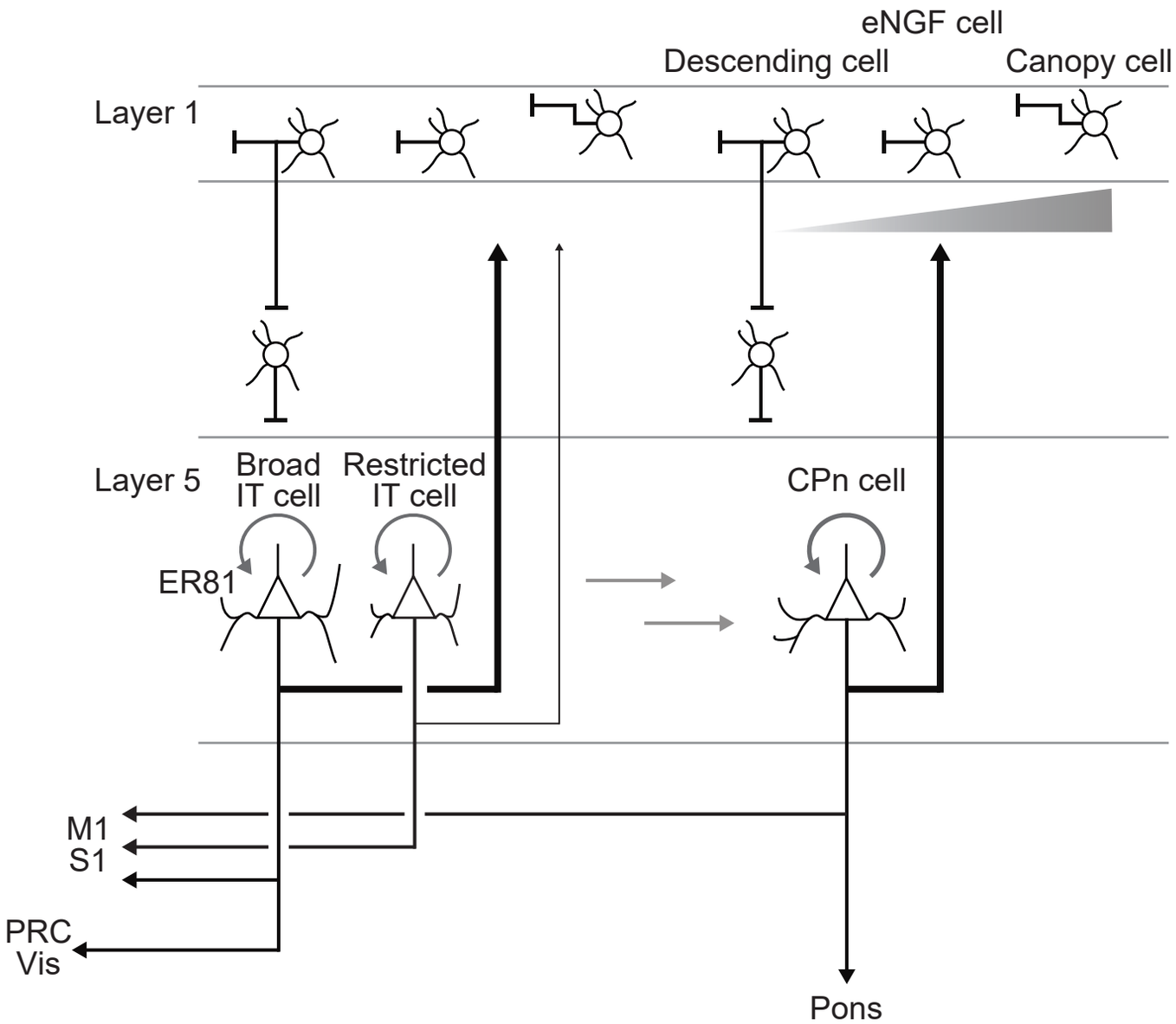

Figure 14. L5 corticocortical cell subtypes and their innervation of L1 cells.

In L5 IT cells, preference for L1 innervation correlates with that for distal cortex projection. CPn cells excite L1 cell subtypes more selectively than L5 IT cells.

Acknowledgments

The dissertation is a part of requirements for receiving the doctor's degree, conferred by SOKENDAI. I would like to express my gratitude to Prof. Yasuo Kawaguchi for the help with the experimental model, the conductance of the research, discussions and encouragements for this research. I would like to thank Dr. Mieko Morishima for the help with the experimental model and Dr. Mohammed Youssef for date analysis. I would like to thank Dr. Kenta Kobayashi for providing the AAV 2.5 CAG Double flox Synaptophysin-EGFP WPRE. I would like to thank Dr. Yuchio Yanagawa and Dr. Ryosuke Kaneko for providing the VGAT-tdTomato mice. I would like to appreciate Chiemi Hyodo for help with mice care.

Finally, I would like to thank my parents, friends and all members of Prof. Kawaguchi's laboratory in NIPS: Yoshiyuki Kubota, Takeshi Otsuka, Yumiko Hatanaka, Jaerin Sohn, Fransiscus Adrian Agahari, Alsayed Abdelhamid Mohamed, Ahmed Abdel-Wahab Mohamed Khalaf, Noboru Yamaguchi, Seiko Watanabe, Sayuri Inuzuka, Naomi Egawa, Nobuko Hattori, Hiroko Kita and Hiromi Ichikawa for the support and encouragement for this research.